Optical Soliton Bistability, Amplification, and Switching

by

Sandra Lee-Anne Eix

B.Sc., University of Waterloo, 1991

THESIS SUBMITTED IN PARTIAL FULFILMENT

OF THE REQUIREMENTS FOR THE DEGREE OF MASTER

OF SCIENCE

IN THE DEPARTMENT OF PHYSICS

Simon Fraser University

May 1993

Approval

NAME: Sandra L. Eix

DEGREE: Master of Science

THESIS TITLE: Optical Soliton Bistability, Amplification, and Switching

EXAMINING COMMITTEE:

Chair : Dr. M.L.W. Thewalt

Dr. R.H. Enns, Senior Supervisor

Dr. S.S. Rangnekar

Dr. K. Rieckhoff

Dr. B. Frisken, External Examiner

Department of Physics, Simon Fraser University

DATE APPROVED : June 7 '93

PARTIAL COPYRIGHT LICENSE

I hereby grant to Simon Fraser University the right to lend my thesis, project or extended essay (the title of which is shown below) to users of the Simon Fraser University Library, and to make partial or single copies only for such users or in response to a request from the library of any other university, or other educational institution, on its own behalf or for one of its users. I further agree that permission for multiple copying of this work for scholarly purposes may be granted by me or the Dean of Graduate Studies. It is understood that copying or publication of this work for financial gain shall not be allowed without my written permission.

Title of (Thesis)/Project/Extended Essay

Optical Soliton Bistability, Amplification, and Switching

Author:

(signature)

Sandra Lee-Anne Eix

(name)

May 31, 1993

(date)

Abstract

Soliton solutions to the generalized nonlinear Schrödinger equation (GNLSE) model the behaviour of light pulses in certain optical fibers. These optical solitons have been the object of much recent interest because of their potential applications in communications technology and in optical computing. In this thesis, the physical phenomena leading to soliton formation are reviewed, and the GNLSE is solved for two models of fiber nonlinearity.

Optical fibers may support bright soliton bistability in two ways. Bistable solitons of the *first* kind (BISOL1) exist when solitons may propagate with the same total energy but different propagation parameters. Bistable solitons of the *second* kind (BISOL2) exist when the fiber supports solitons with the same width but different amplitudes. Two models of fiber nonlinearity are shown to support BISOL2, but not BISOL1, and collisions between BISOL2 are investigated numerically.

Dark solitons are also supported by one of the models under discussion. The solution of the GNLSE for dark solitons is presented and classes of bistability, analogous to those identified for bright solitons, are proposed for dark solitons.

It has been demonstrated previously that it is possible to switch between high and low state BISOL1, by amplifying a soliton pulse. In this thesis, BISOL2 are amplified numerically, and the results are compared to the predictions of a variational analysis based on that of Anderson (Phys. Rev. **A27** (1983) 3135). The variational method generally predicts the observed numerical behaviour well. However, it is

not able to account for the switching that occurs for suitably chosen amplifications. Both upswitching (from low to high state) and downswitching (from high to low state) are demonstrated for two different models of the fiber nonlinearity. In both models, essentially hysteresis-free back-and-forth switching is observed numerically between BISOL2 states, whereas such behaviour is not generally possible for BISOL1. While fibers described by both models allow amplificational switching, those with a saturable nonlinearity are likely to be more useful in practice, as they easily allow switching between solitons of very different amplitudes.

Acknowledgements

My thanks go to Dr. R.H. Enns for suggesting this project and for his support and encouragement throughout its completion. Dr. S.S. Rangnekar and Darran Edmundson provided many useful suggestions. NSERC's generous financial support has also been much appreciated.

I thank my fellow graduate students, who kept me suitably distracted. And last but certainly not least I thank Dave, who never doubted that I could get this far.

Contents

List of Tables

List of Figures

Chapter 1

Introduction

1.1 Solitons and Optical Technology

Optical fibers have been used since the 1970's for communications technology (telephone lines, for example). Information is sent along a fiber in binary form as a series of ones and zeros. Conventionally, a pulse of light is used to represent one and a space is used to represent zero. Several difficulties arise when these light pulses are sent along optical fibers. Fiber loss, due to Rayleigh scattering and absorption, causes the pulses to lose intensity as they travel, and dispersion inherent to the dielectric fiber causes pulse broadening. Loss limits the distance over which information can travel, and dispersion limits the rate at which zeros and ones may be sent.

Originally, these difficulties were overcome by using fibers with very low loss, stationing repeaters in the fibers to reduce the distance that a pulse needs to travel, and using only wavelengths at which the dispersion falls to zero. Now, it is also possible to manufacture fibers with appropriate nonlinear refractive indices, so that the nonlinear effects balance the effects of dispersion. The stable, extremely narrow

pulses (solitons) which may be propagated in such fibers allow for very high bit-rate data transmission over long distances. A model for the physical processes involved is described in section 1.2.

Rather than using pulses and gaps to represent ones and zeros, one could use tall and short pulses. The major advantage of the latter system is that it makes simple switching between zeros and ones conceivable; it may also allow data bits to be sent closer to each other without confusion. Bistability makes it possible to identify "high" and "low" state solitons, and thus offers a way to create tall and short pulses in practice. Two main classes of bistability have been identified in the literature. Bistable solitons of the first kind are those for which the same total energy (or energy deficiency, for dark pulses) is possible for different propagation parameters. Bistable solitons of the second kind have the same width for different amplitudes. Bistability for bright and dark solitons is discussed in detail in Chapters 2 and 3.

A great deal of interest has been shown recently in the possibility of optical computing; that is, applying the technology of fiber optics to logic operations. Logic operations require a mechanism for switching between ones and zeros. As mentioned above, bistable solitons provide a method of coding binary information which allows the possibility of switching. Switching between high and low state bright solitons in systems with bistability of the first kind has been demonstrated by Enns et al. (see [1] and references therein). The amplification and switching of bright bistable solitons

of the second kind are the subjects of Chapters 4 and 5, where both analytical and numerical methods are used to investigate the consequences of amplifying pulses. This work has been accepted for publication in Physical Review [2].

1.2 The Physics of Soliton Propagation

1.2.1 Solitons and the NLSE

The term "soliton" was coined in 1964 by Zabusky and Kruskal [3] to describe solitary wave solutions to the Korteweg/deVries (KdV) equation. Solitary waves are localized, isolated pulses. The solitary waves regained their original shape exactly after colliding or passing through one another, and were given the name "soliton" to reflect their particle-like behaviour. Two years later, in 1967, Gardner et al. [4] used the inverse-scattering method to solve the KdV equation. This method is described in some detail in [5]. In the inverse-scattering solution, solitons are described as bound states of a Schrödinger operator. This description gives a theoretical basis for the particle model of solitons.

The KdV equation was originally derived to describe long wavelength, shallow water waves in a rectangular canal. A different mathematical description is needed for light pulses in fibers, which usually take the form of local modifications to the amplitude of a carrier wave. The propagation of the envelope pulses is governed by the *nonlinear Schrödinger equation* (NLSE) and its generalizations. The NLSE shown below describes the motion of an envelope function $E(z,t)$, which is assumed to vary slowly in space and time relative to the carrier wave, in a lossless fiber with

the Kerr nonlinearity:

$$i\frac{\partial E}{\partial z} - \frac{k''}{2}\frac{\partial^2 E}{\partial \tau^2} + \frac{kn_2}{n_0}|E|^2 E = 0\,. \tag{1.1}$$

Here E represents the amplitude of the electric field, z is the spatial co-ordinate in the direction of motion; $\tau = t - z/v_g$, is a retarded time for group velocity $v_g = d\omega/dk$; $k'' = d^2k/d\omega^2$ is the group velocity dispersion (GVD) where k is the wavenumber of the envelope wave and ω is its frequency; and the index of refraction in the fiber is $n = n_0 + n_2|E|^2$ for the Kerr nonlinearity. The detailed derivation of the NLSE from Maxwell's equations can be found in [5] or [6],but is not included here. Instead, the physical processes behind the NLSE are described.

The propagation of stable solitary waves depends on a balance between the effects of the nonlinearity and the dispersion. In the NLSE the dispersion is governed by the second term and the nonlinearity by the third.

Dispersion

Dispersion exists when the wavenumber, k, of the envelope pulse depends on its frequency, ω. The precise nature of the dependence is determined by the molecular structure of the fiber. The relation $k(\omega)$ can be expressed in terms of the relationship between index of refraction, n, and wavelength, λ, which is tabulated for many dielectrics.

Since $k = n(\omega)\omega/c$ it follows that

$$\frac{dk}{d\omega} = \frac{1}{c}\left[\omega\frac{dn}{d\omega} + n\right]\,.$$

Now, also, $\omega = 2\pi c/n(\lambda)\lambda$, so $dn/d\omega$ can be written:

$$\frac{dn}{d\omega} = \frac{dn/d\lambda}{d\omega/d\lambda}.$$

Using this, the group velocity can be found as follows:

$$\begin{aligned} \frac{1}{v_g} = \frac{dk}{d\omega} &= \frac{1}{c}\left[\frac{n}{1+\frac{\lambda}{n}\frac{dn}{d\lambda}}\right] \\ &\approx \frac{n}{c}\left[1-\frac{\lambda}{n}\frac{dn}{d\lambda}\right] \text{ if } \frac{\lambda}{n}\frac{dn}{d\lambda} \text{ is small}. \end{aligned} \tag{1.2}$$

Similarly,

$$\begin{aligned} \frac{d^2k}{d\omega^2} &= \frac{n\lambda}{2\pi c^2}\left[\lambda^2\frac{d^2n}{d\lambda^2} - \frac{2}{n}\left(\lambda\frac{dn}{d\lambda}\right)^2\right]\left[1+\frac{\lambda}{n}\frac{dn}{d\lambda}\right]^{-3} \\ &\approx \frac{n\lambda}{2\pi c^2}\left(\lambda^2\frac{d^2n}{d\lambda^2}\right) \text{ if } \frac{\lambda}{n}\frac{dn}{d\lambda} \text{ is small} \end{aligned} \tag{1.3}$$

For a wide variety of dielectrics [7], $n(\lambda)$ and $dn/d\lambda$ have the shapes shown in Figure 1.1 , so $d^2n/d\lambda^2$ (and hence k'') is positive for lower wavelengths, zero for some wavelength, and negative for higher wavelengths. Positive k'' is referred to as *normal* dispersion, while negative k'' is referred to as *anomalous* dispersion.

Since, for nonzero dispersion, the wavenumber is dependent on frequency, it follows that phase velocity ($v_{ph} = \omega/k(\omega)$), in general, depends on frequency. Different frequency components of a pulse travel at different speeds. Thus, dispersion causes the pulse to spread as it propagates through the fiber. Pulse spreading is independent of the sign of the group velocity dispersion, and occurs for both dark and bright pulses. Detailed treatments of dispersion can be found in [8] and [9].

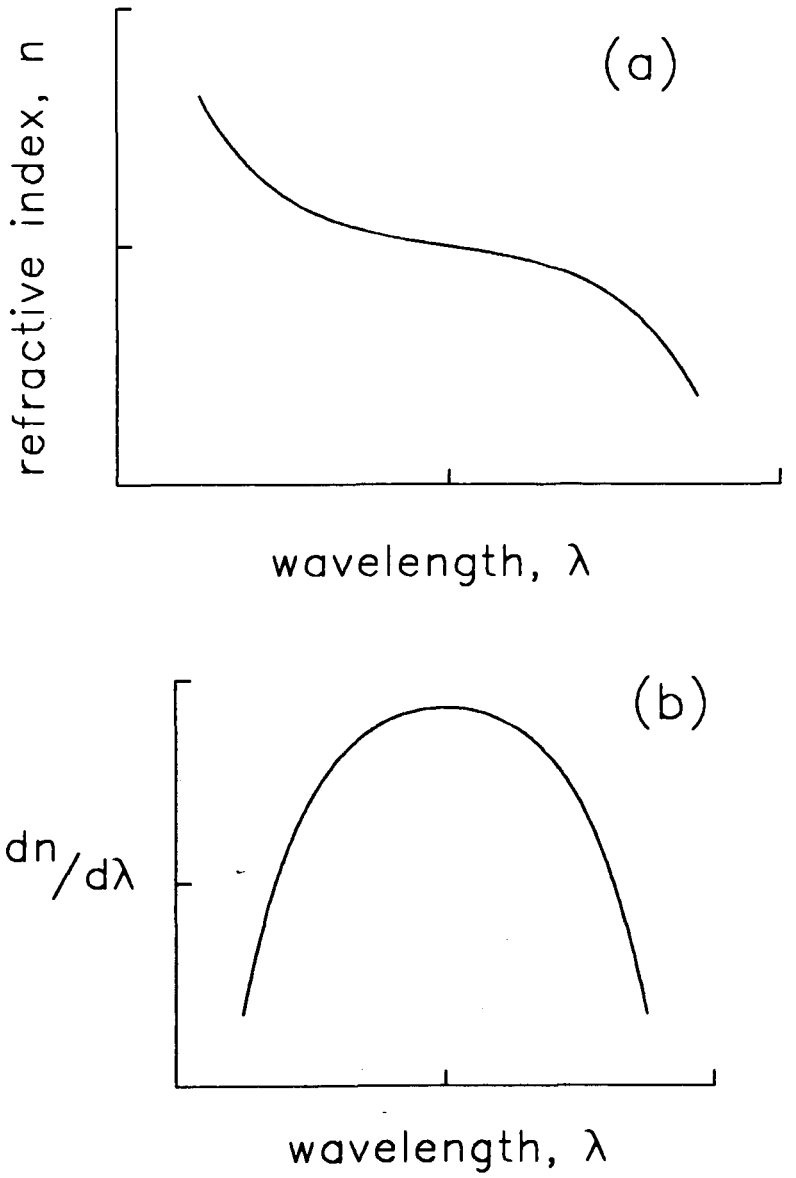

Figure 1.1: Typical shapes of wavelength-dependent refractive index curves
(a) Refractive index vs. wavelength (λ is a log scale).
(b) $dn/d\lambda$ vs. wavelength (log-log plot). The derivative of this function is proportional to the group velocity dispersion.

Nonlinearity

The effects of the fiber nonlinearity can be seen more easily if the dispersion term is removed from the NLSE. The resulting propagation equation is :

$$i\frac{\partial E}{\partial z} + \frac{n_2 k}{n_0}|E|^2 E = 0 \tag{1.4}$$

which has the solution:

$$E(z,\tau) = E(z=0,\tau)\exp(i\frac{n_2 k}{n_0}|E(0,\tau)|^2 z) \tag{1.5}$$

The phase shift is proportional to the pulse intensity, $|E(0,\tau)|^2$, and so is time-dependent. The time dependence of the phase can be expressed as a frequency shift. After time $\delta\tau$, the frequency shift is

$$\begin{aligned} \delta\omega &= \frac{\partial(\text{phase})}{\partial\tau}\delta\tau \\ &= \frac{n_2 k}{n_0}\frac{\partial(|E|^2)}{\partial\tau}\delta\tau \ . \end{aligned} \tag{1.6}$$

For a pulse which is concave down, $\partial(|E|^2)/\partial\tau$ is positive in the trailing part and negative in the leading part, so the trailing part of the pulse is raised in frequency while the leading part is lowered in frequency. If group velocity, $v_g = d\omega/dk$, is an increasing function of frequency (which occurs for $d^2k/d\omega^2 < 0$), the trailing part of the pulse speeds up while the leading part slows down, and the pulse is compressed.

For a concave up pulse, $\partial(|E|^2)/\partial\tau$ is negative in the trailing part and positive in the leading part, so the trailing part is lowered in frequency, while the leading part is raised in frequency. In this case $d^2k/d\omega^2 > 0$ is the necessary condition for pulse compression.

Both the amount of broadening due to dispersion and the amount of compression due to the nonlinearity depend on the initial shape (particularly the width) of the pulse. For some pulse shapes and widths, the two effects can exactly balance one another, allowing the pulse to propagate unchanged. This stable pulse is a soliton.

"Concave down" solitons which take the form of localized pulses of radiation against a zero intensity background are called bright solitons. They are possible in the presence of anomalous dispersion. Solitons which take the form of localized holes in a nonzero intensity background ("concave up") are known as dark solitons, and can exist in the presence of normal dispersion. Dark and bright solitons, with some relevant parameters labelled, are shown in Figure 1.2. In 1973, Hasegawa and Tappert [10, 11] solved the NLSE for both bright and dark solitons. Independently, Zakharov and Shabat used the inverse scattering method to solve the NLSE for bright solitons [12] and dark solitons [13].

1.2.2 Generalization of the NLSE

The NLSE models a fiber with the Kerr nonlinearity; that is, one whose refractive index is described by $n = n_0 + n_2|E|^2$. Many other nonlinearities are possible in practice, depending on the dielectric medium and the intensity of the light being propagated. The generalized nonlinear Schrödinger equation (GNLSE) was developed to allow for various models of refractive index.

If the index of refraction is given by $n = n_0 + n_2 F(|E|^2)$, the GNLSE is written

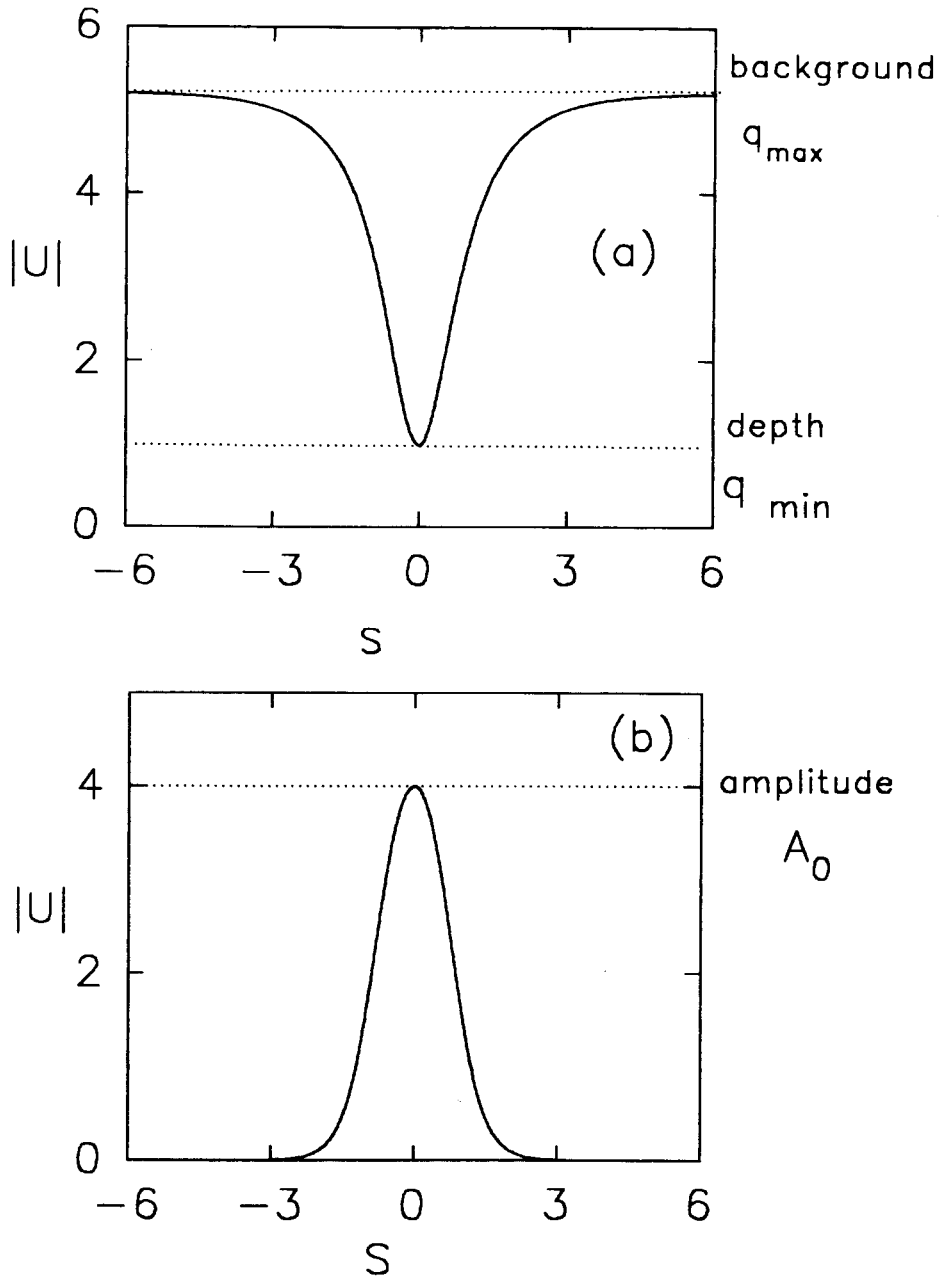

Figure 1.2: Typical shapes of dark and bright solitons, in normalized units given by equation (1.8)

(a) - dark soliton

(b) - bright soliton

as follows:

$$i\frac{\partial E}{\partial z} - \frac{k''}{2}\frac{\partial^2 E}{\partial \tau^2} + \frac{kn_2}{n_0}F(|E|^2)E = 0\,. \tag{1.7}$$

Equation (1.7) reduces to the NLSE if $F(|E|^2) = |E|^2$.

It is conventional to write the GNLSE in normalized units as follows:

$$i\frac{\partial U}{\partial \xi} \pm \frac{1}{2}\frac{\partial^2 U}{\partial s^2} + f(|U|^2)U = 0\,. \tag{1.8}$$

The second term is positive for anomalous dispersion and negative for normal dispersion. The dimensionless quantities used here are $\xi = z/z_L$, $s = \tau/t_0$, and $U = E/\sqrt{P_0}$; where

$$P_0 = \frac{|k''|}{t_0^2|\kappa|}\,,\ z_L = \frac{t_0^2}{|k''|}\,,\ \text{and}\ \kappa = \frac{kn_2}{n_0}\,.$$

The constant $t_0 = \tau_0/1.76$ is the pulse duration (FWHM of $|U|^2$) normalized to the pulse duration of $\text{sech}^2(s)$.

For example, a fiber made of silica glass (SiO_2) has a group velocity dispersion of $k'' = -10\text{ps}^2/\text{km}$ at a wavelength of 1.5 μm. The constant n_2 is known to be approximately $1.22 \times 10^{-22}\text{m}^2/\text{V}^2$ and n_0 is about 1.4 [5]. For a pulse with width $\tau_0 = 5\text{ps}$, a silica fiber has $t_0 \approx 2.8\text{ps}$, $P_0 \approx 3.6 \times 10^{12}\text{V}^2/\text{m}^2$, and $z_L \approx 807\text{m}$. This means that $\xi = 1$ corresponds to a distance of 0.8km, $s = 1$ corresponds to a (retarded) time of 2.8ps, and $U = 1$ corresponds to an electric field strength of about $2 \times 10^6\text{V/m}$. Silica glass has a nonlinear index of refraction of the Kerr form, but these numbers provide a first approximation of the magnitudes of the quantities involved for more complex nonlinearities.

The function $f(|U|^2)$ is related to $F(|E|^2)$ by:

$$f(|U|^2) = \frac{kn_2t_0^2}{|k''|n_0} F(|E|^2) \, . \tag{1.9}$$

Equation (1.8) has been solved (either numerically or analytically) for several different forms of the function f, for both bright [14, 15, 16, 17] and dark [18, 19] solitons. Chapter 2 gives details of the bright soliton solutions for the models $f(I = |U|^2) = I - \alpha I^2$ and $f(I) = \frac{1}{2} I(\gamma I + 2)(1 + \gamma I)^{-2}$, which describes a fiber with a saturable nonlinearity. Chapter 3 outlines the dark soliton solution for $f(I) = I - \alpha I^2$. These models for f were chosen for detailed study because the analytical solutions are known, and because there is reason to believe that real fibers with these nonlinearities can be manufactured. Herrmann [18] gives a possible mechanism which may lead to the nonlinearity $f = I - \alpha I^2$ in semiconductor doped fibers. This nonlinearity has also been used by Puell et al. [20] to account for their observations of laser pulse propagation in Rubidium vapour. Fibers with saturable nonlinearities have been observed by Coutaz and Kull [21].

1.2.3 Notes about Stability

Originally, the term "soliton" referred only to those solitary waves which are absolutely stable against large perturbations, such as collisions. More recently, in the physics literature, the term has come to describe a much wider class of solitary waves which are stable only against weak perturbations. For bright solitons, stability considerations have been studied extensively.

It has been established (see [1] and references therein) that the dependence of the total energy $P = \int_{-\infty}^{\infty} |U|^2 ds$ on the propagation parameter, β, can be used to predict the stability of a pulse of the form $U(\xi, s) = q(s)\exp(i(\beta\xi + \phi))$. For 1,2 or 3 dimensions, $dP/d\beta > 0$ guarantees stability of a solitary wave solution against small perturbations, whereas $dP/d\beta < 0$ indicates an absolutely unstable pulse. Collision and switching studies [1, 22] indicate that solitary waves for which $dP/d\beta > 0$ are also stable against large perturbations when $f(I)$ is Kerr-like ($f \propto I$) for low I, rises like I^n with $n \geq 3$ at intermediate I, and either becomes Kerr-like again or saturates to a constant value at large I. Solutions of the GNLSE for the model $f = I - \alpha I^2$, which are discussed in more detail in following chapters, have been tested for stability by Enns and co-workers [22] and by Sombra [23]. For α either positive or negative, quasi-soliton behaviour can occur; that is, small amounts of radiation are emitted during a collision, but the pulse is stable.

1.3 Experimental Verification of Solitons

The NLSE (1.1) does not take fiber loss into account, although loss has a large impact in experimental investigations of soliton propagation. Loss may be due to absorption or Rayleigh scattering, by fiber imperfections or impurities and by the fiber material itself. If loss is included, the NLSE becomes:

$$i\frac{\partial E}{\partial z} - \frac{k''}{2}\frac{\partial^2 E}{\partial \tau^2} + \frac{kn_2}{n_0}|E|^2 E = -i\Gamma E\,, \tag{1.10}$$

where Γ is known as the loss rate. A soliton can only survive if the nonlinear term is larger than the loss term; otherwise, the pulse will simply vanish before any nonlinear effects can be observed.

Fiber loss depends on wavelength, as does group velocity dispersion. To propagate a soliton experimentally, it is necessary to find a wavelength at which both GVD and loss are small in magnitude, so that the nonlinearity can compensate for both effects. This typically occurs around 1.5μm. For a glass fiber, the constant n_2 is about $1.2 \times 10^{-22}\mathrm{m}^2/\mathrm{V}^2$ and n_0 is between 1 and 3. If the electric field is 10^6 V/m (created by an optical power of 100 mW in a fiber with cross-sectional area 60$\mu\mathrm{m}^2$) at a wavelength of 1.5μm, the nonlinear coefficient, $kn_2|E|^2/n_0$, is on the order of $2\times10^{-4}\mathrm{m}^{-1}$. The loss rate Γ must be less than $2\times10^{-4}\mathrm{m}^{-1}$, or, in terms of power loss per kilometre, the loss must be less than 1.7 dB/km (33 % /km). After Hasegawa and Tappert's prediction of optical solitons, it took several years to develop fibers with losses low enough that the nonlinear term is significant. (Commercially available fibers today have loss rates less than 0.2 dB/km, or 4.5%/km.)

In 1980, Mollenauer, Stolen and Gordon [24] observed bright solitons at a wavelength of 1.55μm in a 700 m long silica glass fiber. In 1987 and 1988, dark solitons were observed by Emplit et al. [25], Krökel et al. [26], and Weiner et al.[27]. Krökel et al. observed the formation of dark solitons from 0.3-psec dark pulses at 532 nm, propagating through 10m of single-mode fiber. Weiner's experiment used 185-fsec. pulses at 620 nm in a 1.4 m length of fiber. All these results compared favourably

with numerical soliton solutions of the NLSE. Very recent experiments have resulted in the error-free transmission of binary information through 9000 km of fiber at a rate of 5 gigabits per second [28]. This was accomplished using erbium doped fiber amplifiers, nonlinear all-optical devices which are located at intervals along the fiber.

Chapter 2

Bright Solitons

2.1 Bright Soliton Solutions of the GNLSE

Bright solitons are possible when the group velocity dispersion ($d^2k/d\omega^2$) is negative, or, in other words, in the presence of anomalous dispersion. Analytical bright soliton solutions to the NLSE have been known since Hasegawa and Tappert's solution in 1973. The *generalized* nonlinear Schrödinger equation (GNLSE) introduced in Chapter 1 may also be solved analytically, for appropriate choices of the nonlinearity.

The GNLSE, for anomalous dispersion, is written in normalized soliton units as follows:

$$i\frac{\partial U}{\partial \xi} + \frac{1}{2}\frac{\partial^2 U}{\partial s^2} + f(|U|^2)U = 0\,. \tag{2.1}$$

If the solution is assumed to have the form

$$U(\xi, s) = q(s)\exp(i\beta\xi + i\phi)\,, \tag{2.2}$$

with q, β, and ϕ real, and the boundary conditions

$$q(s) \to 0 \quad \text{and } dq/ds \to 0 \quad \text{as } s \to \pm\infty \tag{2.3}$$

$$q(s) = A_0 \quad \text{and } dq/ds = 0 \quad \text{at } s = 0\,, \tag{2.4}$$

the GNLSE reduces to

$$\frac{d^2q}{ds^2} + 2(f(q^2) - \beta)q = 0 \,. \tag{2.5}$$

Multiplying by $2(dq/ds)ds$ and integrating once gives

$$\left(\frac{dq}{ds}\right)^2 = 2\int_0^{q^2} (\beta - f(q'^2))\, dq'^2 \,. \tag{2.6}$$

This may also be written

$$\left(\frac{dq}{ds}\right)^2 = 2(\beta q^2 - F(q^2)) \,, \text{ where} \tag{2.7}$$

$$F(q^2) = \int_0^{q^2} f(q'^2)\, dq'^2 \tag{2.8}$$

and it is assumed that $F(0) = 0$.

Applying the boundary condition (2.4) to equation (2.7) gives the following expression for the propagation constant β :

$$\beta = \frac{F(A_0^2)}{A_0^2} \tag{2.9}$$

Integrating equation (2.7) results in an expression relating q and s:

$$s = \int \left[2(\beta q^2 - F(q^2))\right]^{-1/2} dq \,. \tag{2.10}$$

Most often, the integration in equation (2.10) must be performed numerically; however, for some forms of the nonlinearity f, an analytic solution is possible. For example, Enns and co-workers [22], in their studies of bistability, found exact analytic solutions for the "linear + smooth step" nonlinearity

$$f(I) = \begin{cases} \alpha I, & I \le I_0 \\ \Delta[1 - (1-\mu)I_0^2/I^2] & I \ge I_0 \end{cases} \,.$$

The GNLSE with the nonlinearity

$$f(I) = I - \alpha I^2 \tag{2.11}$$

was originally solved by Cowan et al. [17]. Its bright solutions have recently been the subject of much attention from Gatz and Herrmann [18, 29] and Sombra [23]. This form of f corresponds to a refractive index of the form $n = n_0 + n_2|E|^2 + n_4|E|^4$. In normalized soliton units,

$$\alpha = \frac{(1.76)^2 n_4 |k''| k}{\kappa^2 n_0 \tau_0^2} .$$

Gatz and Herrmann propose that this model could be realized experimentally using semiconductor-doped fibers. In [15] and [18] they estimate that for such fibers, α might typically have values near 0.1 for pulses of width near 5ps. If $\alpha = 0$, the nonlinearity described by (2.11) reduces to the Kerr nonlinearity.

Krolikowski and Luther-Davies [16] have recently found analytic solutions for the GNLSE with a saturable nonlinearity described by

$$f = \frac{1}{2} \frac{I(\gamma I + 2)}{(1 + \gamma I)^2} . \tag{2.12}$$

In normalized soliton units,

$$\gamma = \frac{(1.76)^2 |k''|}{\tau_0^2 \kappa I_{\text{sat}}} .$$

I_{sat} is a constant of the model for refractive index, $n = n_0 + \Delta n$, where

$$\Delta n \propto \kappa \left(1 - \frac{1}{(1 + I/I_{\text{sat}})^2} \right) .$$

The latter two models will be the focus of further discussion in this chapter, because of their relatively straightforward solutions.

2.2 Bistable Solitons of the First Kind

Bistable soliton solutions to the generalized nonlinear Schrödinger equation (GNLSE) were first described several years ago by Kaplan, Enns, and co-workers [22, 30]. For certain types of nonlinearity, it was shown that two (or more) solitons could exist with the same energy, $P = \int_{-\infty}^{\infty} |U|^2 \, ds$, but different propagation parameters, β. The energetically degenerate solitons are characterized in general by substantially different amplitudes and widths. These Kaplan-Enns bistable solitons are referred to here as *bistable solitons of the first kind*, or, more succinctly, BISOL1. For BISOL1 to exist, the energy curve obtained when P is plotted against β must be, at least, U-shaped. However, N-shaped $P(\beta)$ curves are more useful for switching applications, since they allow two stable (positive-slope) branches separated by an unstable (negative-slope) region.

It is not necessary to have the complete solution $q(s)$ in order to find $P(\beta)$. Changing the independent variable to $I = q^2$, and using dq/ds given by equation (2.7), the energy can be expressed as:

$$P = \frac{1}{\sqrt{2}} \int_0^{I_{\max}} \frac{dI}{(\beta - I^{-1}F(I))^{1/2}}, \tag{2.13}$$

where $F(I \equiv q^2)$ is defined by equation (2.8) and $I_{\max} \equiv A_0^2$ is related to β by equation (2.9).

For $f = I - \alpha I^2$,

$$\sqrt{\frac{2|\alpha|}{3}} P = \ln \left[\frac{\sqrt{1 - 16|\alpha|\beta/3}}{1 - \sqrt{16|\alpha|\beta/3}} \right] \text{ with } \alpha > 0 \text{ , and} \tag{2.14}$$

$$\sqrt{\frac{2|\alpha|}{3}}P = \frac{\pi}{2} - \arcsin\left[\frac{1}{\sqrt{16|\alpha|\beta/3+1}}\right] \text{ with } \alpha < 0\,. \qquad (2.15)$$

Plots of these relations $P(\beta)$, which were originally derived in [22], are shown in Figure 2.1. It is clear from the plots that β is not double-valued in P, so bistability of the first kind is not possible for $f = I - \alpha I^2$, with α either positive or negative.

In general, the shape of the $P(\beta)$ curve can be deduced from the form of the nonlinearity. For an intensity (I) dependent nonlinearity of the form $f = I^n$ with $n \geq 0$, it has been shown [31] in d-dimensions that $dP/d\beta$ is positive for $n < 2/d$, zero for $n = 2/d$, and negative for $n > 2/d$. For $d = 1, 2, \text{and } 3$ the critical (zero slope) value of n is $2, 1$, and $2/3$, respectively. Thus, bistability is possible for $f(I)$ which are dominated by different n values in different ranges of I. For example, since the negative sign changes the sign of the slope, an N-shaped $P(\beta)$ curve is possible in one dimension for $f(I) = a_1 I + a_2 I^3 - a_3 I^5$ if the positive coefficients a_1, a_2, and a_3 are suitably adjusted [22].

On the other hand, for the saturable model described by equation (2.12), $f \sim I$ at small I, and $f \sim$ constant at large I. Using the analysis above, this means that $n = 1$ at small I and $n = 0$ at large I, so that $dP/d\beta$ does not change sign. BISOL1 are thus not possible for this saturable model.

2.3 Bistable Solitons of the Second Kind

Very recently, Gatz and Herrmann [18, 29] have introduced an alternate definition of bistability. According to their definition, bistable solitons have the same pulse

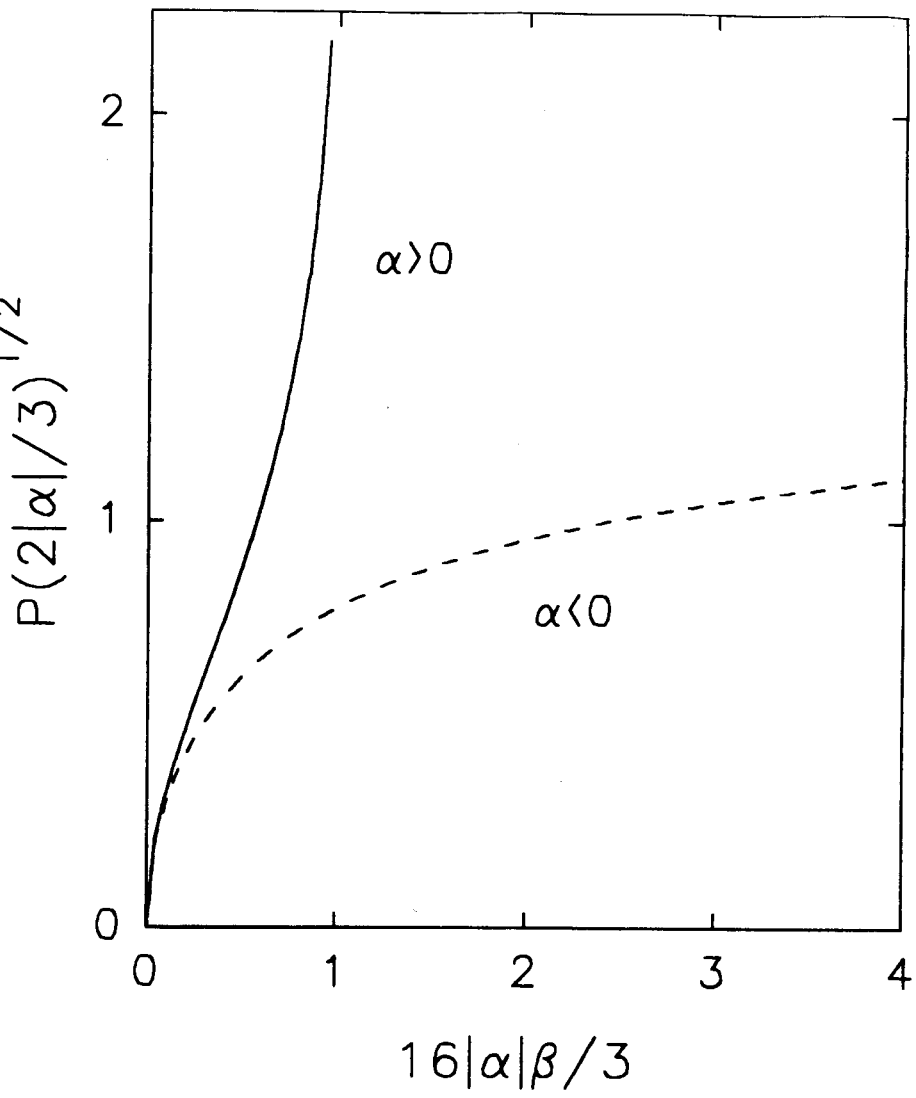

Figure 2.1: Energy vs. propagation parameter for $f = I - \alpha I^2$. The single- valued $\beta(P)$ curve indicates the absence of BISOL1.

duration, τ_0, but different amplitudes, A_0. To avoid confusion with the original definition, the Gatz-Herrmann bistable solitons are referred to as *bistable solitons of the second kind*, or BISOL2. Gatz and Herrmann showed that BISOL2 are possible in one dimension for $f = I - \alpha I^2$ with $\alpha > 0$.

To determine whether BISOL2 exist for a given model, it is necessary to find the form of the soliton solution. Gatz and Herrmann [18, 29] found it convenient to solve the GNLSE using the initial assumption

$$U(\xi, s) = \sqrt{I(s)} \exp(i\beta\xi). \tag{2.16}$$

For the case $f = I - \alpha I^2$, the GNLSE can be solved to obtain:

$$I(s) = \frac{4\beta}{1 + (1 - \frac{4\alpha}{3} I_0) \cosh(2s\sqrt{2\beta})} \tag{2.17}$$

with the propagation parameter $\beta = \frac{1}{2} I_0 (1 - \frac{2}{3}\alpha I_0)$, where

$\sqrt{I_0} = \sqrt{I(s=0)} = A_0$ is the soliton amplitude.

The normalization of t_0 to the pulse duration of $\mathrm{sech}^2(s)$ (see Section 1.2.2) requires that the FWHM of the soliton be that of the function $\mathrm{sech}^2(s)$, approximately 1.76. That is,

$$|U(s = 0.88)|^2 = \frac{1}{2}|U(s = 0)|^2 \tag{2.18}$$

$$\text{or } I(s = 0.88) = \frac{1}{2} I_0 \,. \tag{2.19}$$

Applying this condition to equation (2.17) gives the transcendental equation

$$\cosh\left(1.76\sqrt{A_0^2\left(1 - \frac{2}{3}\alpha A_0^2\right)}\right) = \frac{3 - \frac{8}{3}\alpha A_0^2}{1 - \frac{4}{3}\alpha A_0^2} \tag{2.20}$$

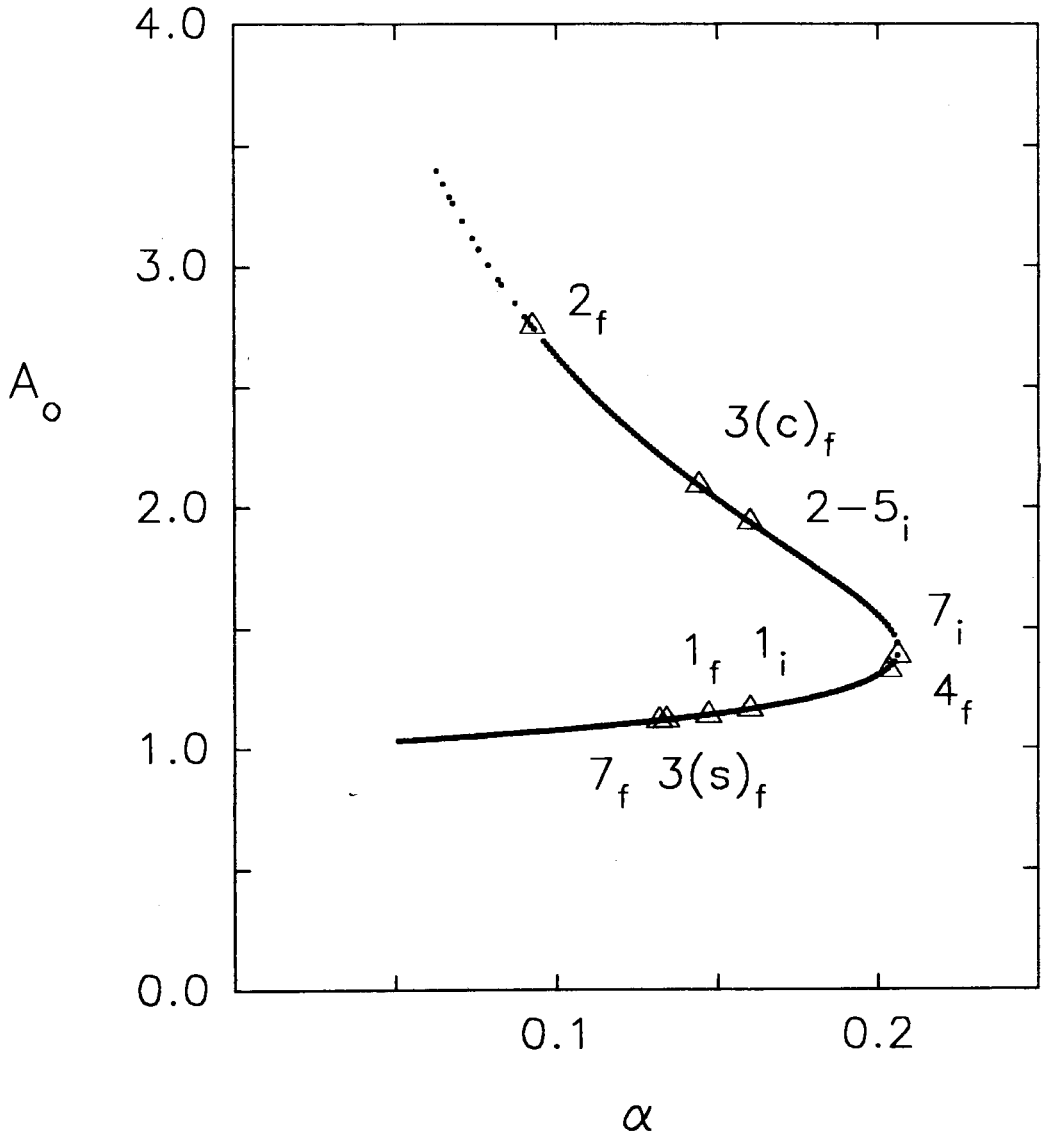

Figure 2.2: Amplitude vs. parameter α for $f = I - \alpha I^2$ with collision results shown
solid line – soliton line given by equation (2.20)
$\triangle$ – initial and final pulses from collision experiments (see Table 2.1)

which defines the relationship between the soliton amplitude A_0 and the parameter α. For fixed material parameters, α depends on the pulse duration ($\alpha \propto \tau_0^{-2}$). The soliton line $A_0(\alpha)$ given implicitly by equation (2.20) is shown in Figure 2.2. Over a certain range of α, the relation $A_0(\alpha)$ is double-valued. Physically, this means that the fiber described by the nonlinearity (2.11) can support solitons with the same width ($\tau_0 \propto \alpha^{-2}$) but with different amplitudes A_0. These are the bistable solitons of the second kind (BISOL2) introduced by Herrmann [14, 18].

For the model described above, the function f reaches a maximum at $I = 1/2\alpha$ and then decreases, eventually becoming negative. Models with other forms also support BISOL2. For example, Krolikowski and Luther-Davies [16] have recently found an analytic solution to the GNLSE (2.1) with a saturable nonlinearity of the form given by equation (2.12). The solution for a different saturable model is given in [14].

Using the assumption (2.16), Krolikowski and Luther-Davies obtained the following relation to describe the soliton solution:

$$2\tan^{-1} Z + \frac{1}{\sqrt{\gamma I_0}} \log\left(\frac{Z+\sqrt{\gamma I_0}}{Z-\sqrt{\gamma I_0}}\right) = s\frac{2}{\sqrt{\gamma^2 I_0 + \gamma}} \tag{2.21}$$

where

$$Z = \left(\frac{I_0 - I}{\gamma^{-1} + I}\right)^{1/2} \quad \text{and } I_0 = I(s=0)\,. \tag{2.22}$$

Applying the half width condition (2.18) gives the following transcendental equa-

tion for the relationship between I_0 and γ:

$$2\tan^{-1}\left(\frac{\gamma I_0}{2+\gamma I_0}\right)^{1/2}+\frac{1}{\sqrt{\gamma I_0}}\log\left(\frac{\sqrt{2+\gamma I_0}+1}{\sqrt{2+\gamma I_0}-1}\right)=\frac{1.76}{\sqrt{\gamma^2 I_0+\gamma}}\,. \qquad (2.23)$$

The relation $I_0(\gamma)$ defined implicitly by equation (2.23) is shown in Figure 2.3. I_0 is double-valued in γ, so BISOL2 exist for this model. It should be noted that Figure 2.2 has $A_0(=\sqrt{I_0})$ on the vertical axis, while Figure 2.3 has I_0.

2.4 Numerical Scheme and Collision Results

Numerical simulations have often been used to study collisions between soliton solutions of the NLSE and the GNLSE [15, 17, 22, 23, 29, 32]. Collisions reveal details of the stability of the solitons, and suggest other behaviour, such as splitting or switching.

Gatz and Herrmann [18, 29] have studied the BISOL2 arising from the model $f = I - \alpha I^2$ in depth. In reference [29], they describe a series of numerical collision experiments. These results are confirmed here both as a demonstration of some of the possible outcomes of soliton collisions, and also as a demonstration of the viability of the numerical scheme used for the switching experiments in Chapter 5.

A three-step explicit scheme was used to simulate the GNLSE numerically. For longer runs, the split-step Fourier algorithm [1] can be used. Gatz and Herrmann used the latter, faster algorithm [29]. In the explicit scheme, a central difference approximation was used for all ξ steps except the first, where a forward difference approximation was required. The forward difference approximation is less accurate

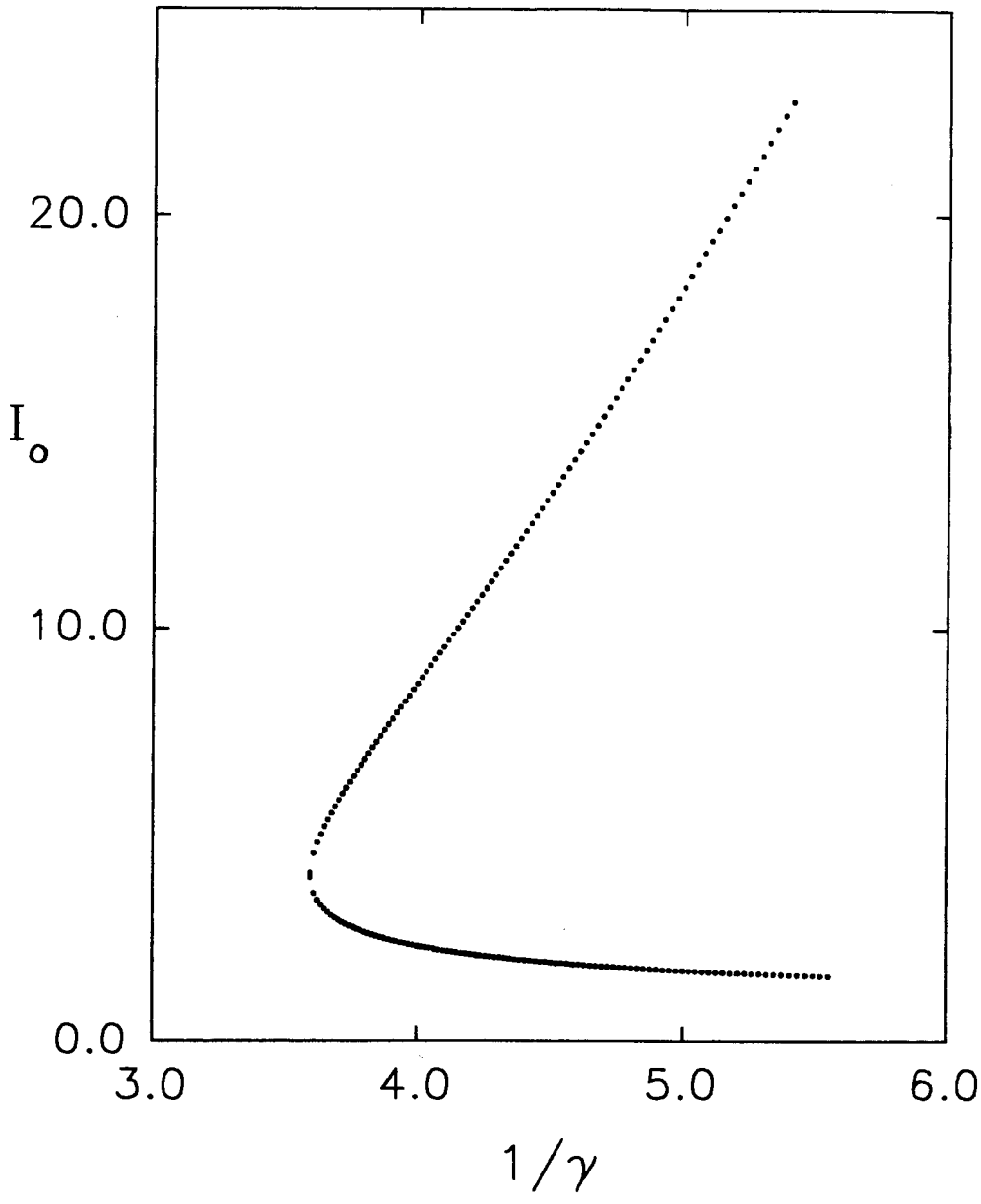

Figure 2.3: Intensity I_0 vs. parameter γ for the saturable model

and becomes numerically unstable after a certain number of ξ steps. This scheme is described in more detail in reference [22]. Typically, the mesh used had $\Delta s \approx 0.1$ and $\Delta\xi \approx 0.001$. To check the accuracy of the numerical runs, and to determine an appropriate step size, the energy integral $P = \int_{-\infty}^{\infty} I\,ds$ was monitored for invariance. The s and ξ step sizes were also varied over two orders of magnitude to check for artifacts related to the mesh size.

For each collision experiment, points were chosen from the soliton line (2.20), and used to form an input function $U(s, \xi = 0)$ of the following form:

$$U(s,\xi=0) = U_1(s-s_0,0)\exp(i\Omega(s-s_0)) + U_2(s+s_0,0)\exp(-i\Omega(s+s_0)) \quad (2.24)$$

U_1 and U_2 are given by equation (2.16) and either (2.17), with A_0 and α chosen to satisfy (2.20), or (2.21), with A_0 and γ chosen to satisfy (2.23). s_0 is a time delay; the pulses begin separated by a time $2s_0$, which must be large enough that the tails of the pulses do not overlap to any significant degree. Ω represents a frequency shift. Because of the anomalous group dispersion, a positive frequency shift causes a pulse to move more quickly, while a negative frequency shift causes a pulse to be slowed down. The delayed pulse, U_1, catches up to and collides with U_2, over the course of the numerical experiment.

Some representative numerical runs are shown in Figures 2.4 and 2.6, along with the corresponding runs from reference [29].

In many of the collision runs, solitary waves emerged after the collision. To determine whether these were solitons, it was necessary to fit them onto the soliton

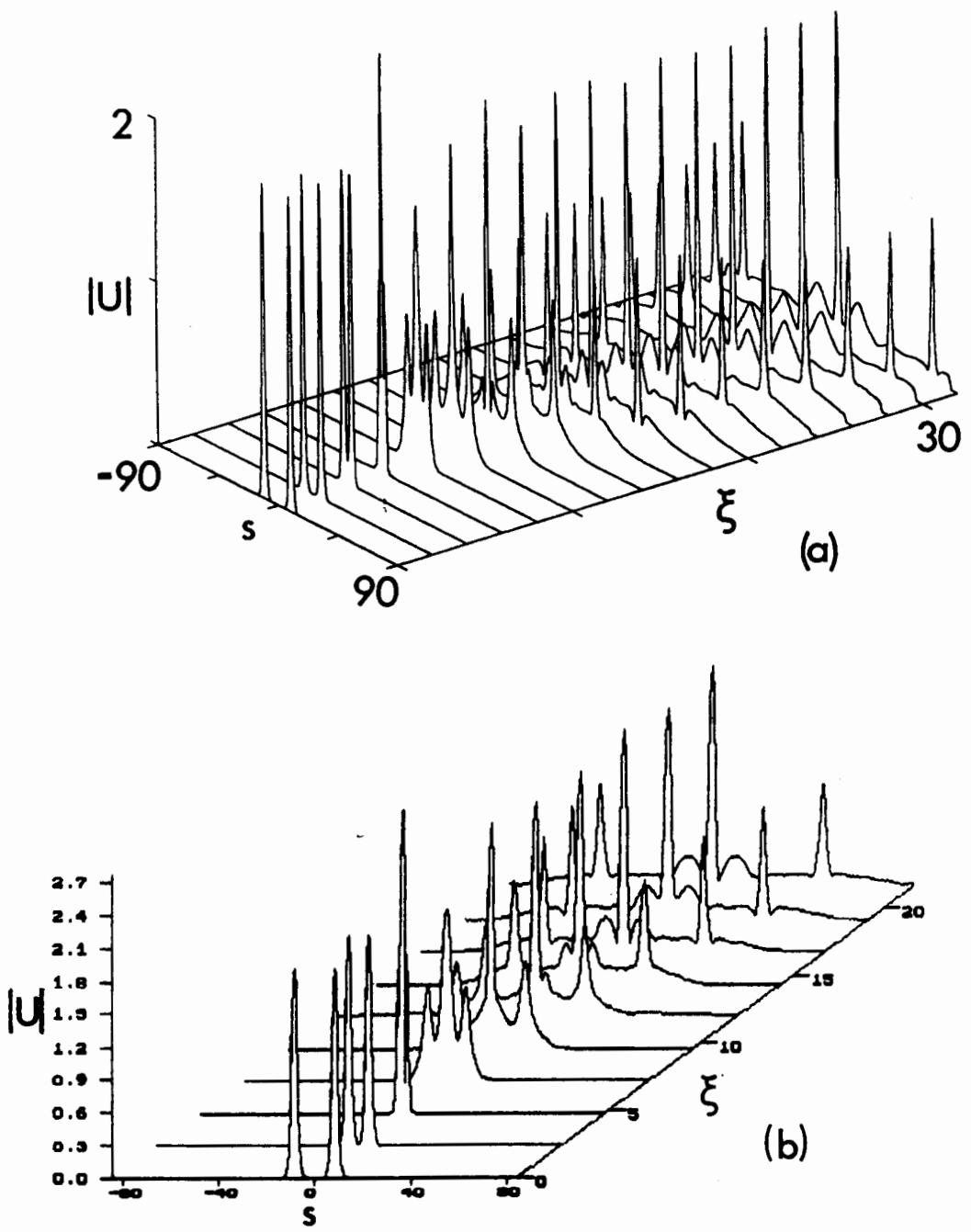

Figure 2.4: (a) Collision run 3 (see Table 2.1 and Figure 2.2)
(b) Corresponding run from [29]

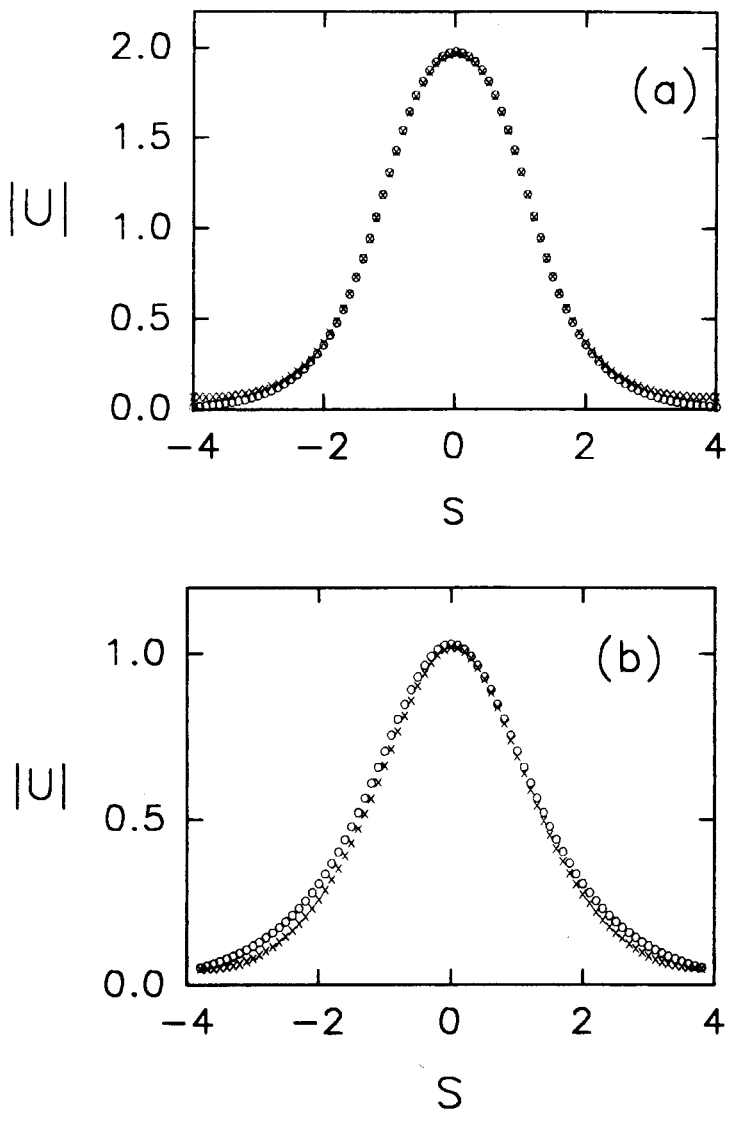

Figure 2.5: Least squares fits of the output pulses from collision run 3
(a) – centre pulse ; (b) – side pulse, located at $s = \pm 71.4$
x – numerical result
o – best fit soliton

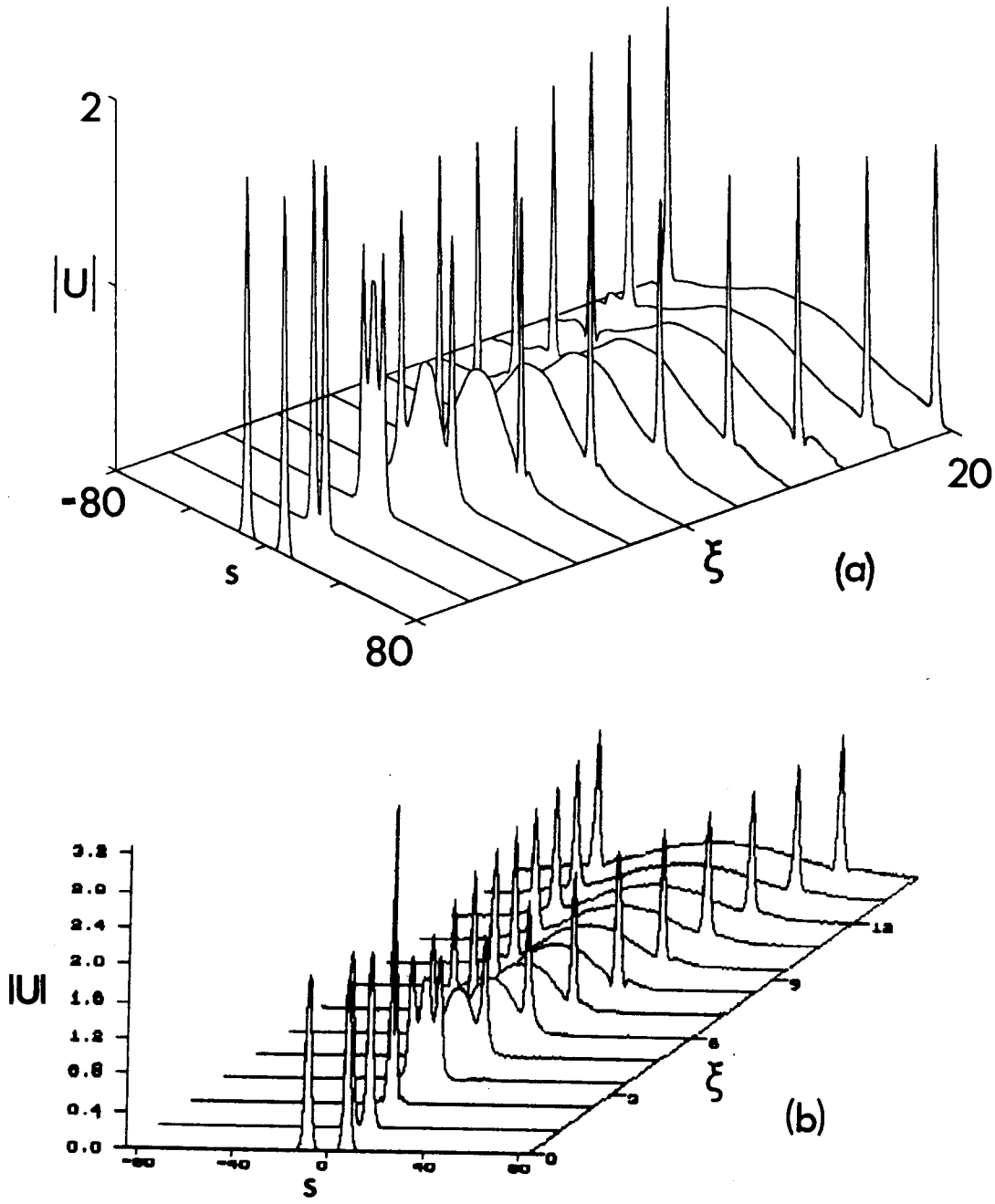

Figure 2.6: (a) Collision run 4 (see Table 2.1 and Figure 2.2)
(b) Corresponding run from [29]

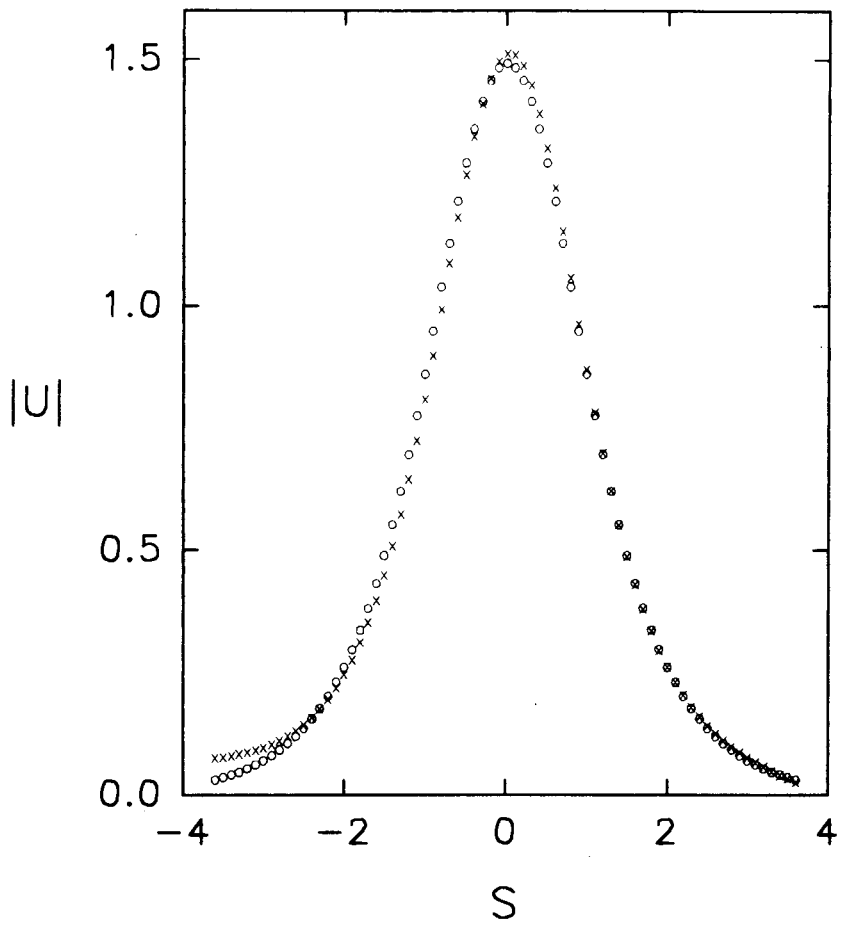

Figure 2.7: Least squares fit of the output pulse from collision run 4, located at $s = \pm 72.0$

x – numerical result

o – best fit soliton

line given by equation (2.20). The process of finding α and A_0 to fit the output pulse has two steps. First, a least squares fit is performed, varying β in equation (2.17) to obtain a best fit equation $I(s)$ for the output pulse. As can be seen in Figures 2.5 and 2.7, the least squares fit is quite accurate.

Second, the pulse is fitted onto the soliton curve (2.20). In order that this can be done, the dimensionless units must be rescaled so that the FWHM of the pulse obtained by the least squares fit is 1.76. Rescaling is accomplished by changing the time scale to $t_0' = \epsilon t_0$, where $\epsilon = \tau_0'/1.76$ and τ_0' is the FWHM of the best fit function $I(s)$. Using the new time scale and the defining relations for α and A_0 we can find scaled values α' and A_0' from the constant α and best fit A_0 as follows:

$$\alpha' = \frac{\alpha}{\epsilon^2}, \quad A_0' = \epsilon A_0 \,. \tag{2.25}$$

These rescaled values α' and A_0' characterize a pulse with FWHM = 1.76, which lies on the soliton line (2.20).

The results of the collision experiments are summarized in Table 2.1, where the results from the three-step explicit scheme are compared to those from reference [29].

The input and output solitons are also indicated in Figure 2.2. The results of the collision experiments done using the explicit scheme are qualitatively the same. The sole exception is run 6, where, in the explicit scheme, the pulses disintegrate into a large number of sharp spikes. The disintegration could be due to the fact that, during the collision, the resulting pulses have amplitudes large enough that $f = I - \alpha I^2$ becomes negative. Parts of the pulses are subjected to the negative nonlinearity, and

the explicit scheme magnifies the resulting instabilities. This difficulty is discussed further in Chapter 4.

Table 2.1: Some representative results of collision experiments for the model $f = I - \alpha I^2$. (s)- side peak. (c)- central peak. See also Figure 2.2

	Input Parameters					Output Parameters			
	ref. [29]		explicit scheme			ref. [29]		explicit scheme	
	α_i	A_{0i}	α_i	A_{0i}	Ω	α_f	A_{0f}	α_f	A_{0f}
1	0.16	1.17	0.1600	1.6566	0.530	0.14	1.12	0.1471	1.1396
2	0.16	1.90	0.1600	1.9388	0.704	0.10	2.62	0.09241	2.7542
3	0.16	1.90	0.1600	1.9388	1.760	(s) 0.12	1.10	0.1340	1.1195
						(c) 0.18	1.75	0.1440	2.0935
4	0.16	1.90	0.1600	1.9388	3.520	(s) 0.21	1.33	0.2033	1.3259
						central peak is not a soliton			
5	0.16	1.90	0.1600	1.9388	5.280	neither peak is a soliton			
6	0.02	6.12	0.0200	6.1207	1.760	0.01	9.87	pulses collide	
						0.08	1.02	and disintegrate	
7	0.21	1.38	0.2060	1.3877	1.760	(s) 0.15	1.15	0.1318	1.1164
						central peak is not a soliton			

Several difficulties arose in the attempt to repeat the quantitative results of [29]. First, the input parameters quoted in [29] are rounded off to two decimal places, but the rounded values do not fit on the soliton line exactly. For the explicit scheme, parameters were chosen from the soliton line to at least four decimal places. Since the output parameters are sensitively dependent on the input α and A_0 values, the output parameters from the explicit scheme runs do not match those from the runs in [29]. This problem is particularly noticeable in run 7.

Second, it is not clear in [29] at what point the output profile is measured. In run 3, particularly, the pulse continues to evolve for greater values of ξ than are

shown in the diagram in [29]. The difference in endpoint can account for some of the discrepancy between the quantitative results of [29] and those of the explicit scheme.

Overall, it is possible to conclude that the explicit scheme is capable of reproducing the results obtained using the more sophisticated split-step Fourier method, for the ranges of s and ξ, and the step sizes chosen here.

Chapter 3

Dark Solitons

3.1 Dark Soliton Solutions of the GNLSE

As was explained in Chapter 1, dark solitons can propagate in fibers with normal dispersion ($d^2k/d\omega^2 > 0$) and a nonlinear index of refraction. Dark soliton solutions to the NLSE have been familiar since Hasegawa and Tappert's work in 1973. The more recent dark soliton solution to the *generalized* nonlinear Schrödinger equation (GNLSE) is presented here.

The GNLSE is written as follows, for normal dispersion and in the normalized units introduced in Chapter 1:

$$i\frac{\partial U}{\partial \xi} - \frac{1}{2}\frac{\partial^2 U}{\partial s^2} + f(|U|^2)U = 0 \tag{3.1}$$

A stationary dark soliton solution of the GNLSE may be assumed to have the form

$$U(\xi, s) = q(s)\exp(i\beta\xi + i\theta(s)) \tag{3.2}$$

(with q, β, θ real) and to satisfy the boundary conditions

$$q \to q_{\max} \quad \text{and } d^2q/ds^2 \to 0 \quad \text{as } |s| \to \infty \tag{3.3}$$

$$q \to q_{max} \quad \text{and } dq/ds \to 0 \quad \text{as } |s| \to \infty \tag{3.4}$$

$$q = q_{min} < q_{max} \quad \text{and } dq/ds = 0 \quad \text{at } |s| = 0 \tag{3.5}$$

A soliton with this form is shown in Figure 1.2(a).

Substituting the form (3.2) for $U(\xi, s)$ into the GNLSE (3.1) gives a system of differential equations in q and θ, as follows:

$$\frac{d^2q}{ds^2} = q\left(\frac{d\theta}{ds}\right)^2 - 2\beta q + 2f(q^2)q \tag{3.6}$$

$$\frac{dq}{ds}\frac{d\theta}{ds} + \frac{1}{2}q\frac{d^2\theta}{ds^2} = 0 \tag{3.7}$$

Equation (3.7) can be integrated to obtain

$$\frac{d\theta}{ds} = \frac{C_1}{q^2}\,, \tag{3.8}$$

where C_1 is a constant of integration. By substituting the above form for $d\theta/ds$ in (3.6), the following equation can be obtained:

$$\frac{d^2q}{ds^2} = \frac{C_1^2}{q^3} - 2\beta q + 2f(q^2)q\,. \tag{3.9}$$

Multiplying equation (3.9) by $2\frac{dq}{ds}ds$ and integrating once gives

$$g(q) \equiv \left(\frac{dq}{ds}\right)^2 = \frac{-C_1^2}{q^2} - 2\beta q^2 + 2\int f(q^2)d(q^2) + C_2\,, \tag{3.10}$$

where C_2 is a second integration constant. The form of $q(s)$ can be found by integrating:

$$\int \frac{dq}{\sqrt{g(q)}} = s + C_3\,, \tag{3.11}$$

where C_3 is another integration constant.

Obviously, the full solution of the GNLSE depends on the form of $g(q)$, and thus on the form of the nonlinearity $f(I \equiv q^2)$. Enns and Mulder [19, 33], for example, developed solutions for a split-Kerr model

$$f = \begin{cases} \beta I & I > I_0 \\ \alpha I & I < I_0 \end{cases}$$

and for the model $f = \Delta I\,[1 + \alpha \tanh[\gamma(I^2 - I_0^2)]]$. The model

$$f = I - \alpha I^2 \tag{3.12}$$

which may describe the behaviour of a real nonlinear fiber, is the focus of more detailed mathematical analysis in the rest of this chapter.

Substitution of $f(q^2 = I)$ given by equation (3.12) leads to the following forms for equations (3.10) and (3.6):

$$g(q) = \left(\frac{dq}{ds}\right)^2 = \frac{-C_1^2}{q^2} - 2\beta q^2 + q^4 - \frac{2}{3}\alpha q^6 + C_2 \tag{3.13}$$

$$\frac{d^2q}{ds^2} = \frac{C_1^2}{q^3} - 2\beta q + 2q^3 - 2\alpha q^5 \tag{3.14}$$

The boundary conditions on q can now be used to obtain the constants β , C_1^2, and C_2. First, when boundary condition (3.3) is applied to equation (3.14), the result is:

$$0 = \frac{C_1^2}{q_{\max}^3} - 2\beta q_{\max} + 2q_{\max}^3 - 2\alpha q_{\max}^5.$$

It is convenient to introduce some new notation. $I = q^2$ is the intensity of the pulse, with $I_{\max} = q_{\max}^2$ and $I_{\min} = q_{\min}^2$. The above equation then simplifies to:

$$C_1^2 = 2I_{\max}^2(\beta - I_{\max} + \alpha I_{\max}^2). \tag{3.15}$$

Next, applying boundary condition (3.4) and the same new notation, equation (3.13) becomes

$$C_1^2 = -2\beta I_{\max}^2 + I_{\max}^3 - \frac{2}{3}\alpha I_{\max}^4 + C_2 I_{\max}. \tag{3.16}$$

Finally, applying the boundary condition (3.5) to equation (3.13) gives

$$C_1^2 = -2\beta I_{\min}^2 + I_{\min}^3 - \frac{2}{3}\alpha I_{\min}^4 + C_2 I_{\min}\,. \tag{3.17}$$

The system of three equations (3.15), (3.16), and (3.17) can be solved for the unknown constants:

$$\beta = \frac{-1}{3}\alpha I_{\min}^2 - \frac{2}{3}\alpha I_{\min} I_{\max} + \frac{1}{2} I_{\min} + I_{\max} - \alpha I_{\max}^2 \tag{3.18}$$

$$C_2 = \frac{1}{3} I_{\max}[-4\alpha I_{\min}^2 - 8\alpha I_{\min} I_{\max} + 6 I_{\min} - 4\alpha I_{\max}^2 + 3 I_{\max}] \tag{3.19}$$

$$C_1^2 = I_{\min} I_{\max}^2 [1 - \frac{2}{3}\alpha I_{\min} - \frac{4}{3}\alpha I_{\max}]\,. \tag{3.20}$$

Now, in terms of I, equation (3.11) can be written

$$\int \frac{dI}{\sqrt{Ig(I)}} = 2s + C_3 \tag{3.21}$$

where, in this case,

$$Ig(I) = -C_1^2 - 2\beta I^2 + I^3 - \frac{2}{3}\alpha I^4 + C_2 I. \tag{3.22}$$

Upon substitution for β, C_1^2 and C_2, $Ig(I)$ can be factored to give

$$\int \frac{dI}{\sqrt{1/3(I_{\max} - I)^2 (I - I_{\min})[3 - \alpha(2I_{\min} + 4I_{\max} + 2I)]}} = 2s + C_3 \tag{3.23}$$

which has the solution:

$$\sqrt{\frac{3}{\eta}} \ln \left[\frac{2\eta^{1/2}[\eta - 2\alpha(I_{\max} - I)^2 - (3 - 8\alpha I_{\max})(I_{\max} - I)]^{1/2}}{(I_{\max} - I)} \right.$$

$$-\frac{(3-8\alpha I_{\max})(I_{\max}-I)-2\eta}{(I_{\max}-I)}\Bigg] = 2s + C_3 \tag{3.24}$$

with

$$\eta = 3(I_{\max} - I_{\min}) - 2\alpha(3I_{\max}^2 - I_{\min}^2 - 2I_{\min}I_{\max}) \,. \tag{3.25}$$

C_3 can be determined by setting $I = I_{\min}$ at $s = 0$:

$$C_3 = \sqrt{\frac{3}{\eta}} \ln[3 - 4\alpha(I_{\min} + I_{\max})] \,. \tag{3.26}$$

Substituting this value for C_3 into the solution (3.24), and solving for I, gives

$$I = I_{\max} - \frac{2\eta}{(3-8\alpha I_{\max}) + (3-4\alpha(I_{\min}+I_{\max}))\cosh(2s\sqrt{\frac{\eta}{3}})} \tag{3.27}$$

At this point, the phase, θ, can also be calculated from equation (3.8). The calculation is not included here, since equation (3.27) provides all the information necessary to discuss bistability of dark solitons.

3.2 Analogue of BISOL1 for Dark Solitons

Chapter 2 describes two classes of bistability for bright solitons. There are BISOL1, solitons with the same energy $P_{\text{bright}} = \int_{-\infty}^{\infty} |U|^2 ds$ but different propagation parameters, and BISOL2, solitons with the same width but different amplitudes. It is possible to develop definitions of bistability for *dark* solitons which are analogous to these.

In 1989, Mulder and Enns [19, 33] developed the first definition of bistability for dark solitons. They defined a "hole energy", which can be thought of as the energy

deficiency in a constant intensity background, due to the dark pulse. It is given by

$$P_{\text{hole}} = \int_{-\infty}^{\infty} (q_{\text{max}}^2 - q^2) ds \ , \tag{3.28}$$

and can also be calculated directly from $g(q)$ (equation (3.13)) as follows:

$$P_{\text{hole}} = 2 \int_{q_{\text{min}}}^{q_{\text{max}}} \frac{(q_{\text{max}}^2 - q^2)}{\sqrt{g(q)}} dq \ . \tag{3.29}$$

The parameters q_{max} and q_{min} are defined in equations (3.3)–(3.5).

If the dimensionless parameter

$$D = \frac{q_{\text{max}}^2 - q_{\text{min}}^2}{q_{\text{max}}^2} = \frac{I_{\text{max}} - I_{\text{min}}}{I_{\text{max}}}$$

is used to describe the hole modulation depth, bistability can be said to occur when more than one value of D corresponds to a given value of P_{hole}; that is, when, for a given background (I_{max}) there are two or more holes of different depths (I_{min}) with the same energy. This is analogous to the Kaplan and Enns [22, 30] definition of bistability for bright solitons (BISOL1).

For the particular nonlinearity modeled by $f = I - \alpha I^2$, it is convenient to write P_{hole} in terms of $I = q^2$:

$$P_{\text{hole}} = \int_{I_{\text{min}}}^{I_{\text{max}}} \frac{I_{\text{max}} - I}{\sqrt{I g(I)}} dI \ , \tag{3.30}$$

where $Ig(I)$ is given by (3.22).

Substituting the full forms of C_1^2, β, and C_2 in equation (3.30), and evaluating the integral gives:

$$P_{\text{hole}} = \pm \sqrt{\frac{3}{2\alpha}} \arccos \left(\frac{8\alpha I_{\text{max}} - 3}{4\alpha(I_{\text{max}} + I_{\text{min}}) - 3} \right) \tag{3.31}$$

where the negative sign is taken for $\alpha(I_{\min} + I_{\max}) > 3/4$. In terms of the dark pulse parameter D, P_{hole} can be written:

$$P_{\text{hole}} = \pm\sqrt{\frac{3}{2\alpha}} \arccos\left(\frac{8\alpha I_{\max} - 3}{4\alpha I_{\max}(2 - D) - 3}\right) . \tag{3.32}$$

From Figure 3.1 it can be seen that the relation $D(P_{\text{hole}})$ is single-valued, so that this model does not support bistability in the sense described above.

3.3 Analogues of BISOL2 for Dark Solitons

It is natural to ask next whether a definition of bistability for dark solitons can be developed which is analogous to BISOL2 for bright solitons. In fact, there are several such definitions, three of which are outlined in this section for the model described by $f = I - \alpha I^2$.

All three definitions begin with finding the soliton line. For bright BISOL2, the soliton line is found using equation (2.18), which expresses a condition on the width of a pulse required by the normalization of soliton units. The analogous condition for dark solitons is:

$$I_{\min} + \frac{1}{2}(I_{\max} - I_{\min}) = I(s = 0.88) \tag{3.33}$$

$$\text{or } \frac{1}{2}(I_{\min} + I_{\max}) = I(s = 0.88) \tag{3.34}$$

Applied to equation (3.27), this condition leads to a transcendental relationship between the background, $I_{\max}$, the minimum intensity $I_{\min}$ and the parameter α:

$$(3 - 8\alpha I_{\max}) + (3 - 4\alpha(I_{\min} + I_{\max}))\cosh\left(1.76\sqrt{\frac{\eta}{3}}\right) = \frac{4\eta}{(I_{\max} - I_{\min})} \tag{3.35}$$

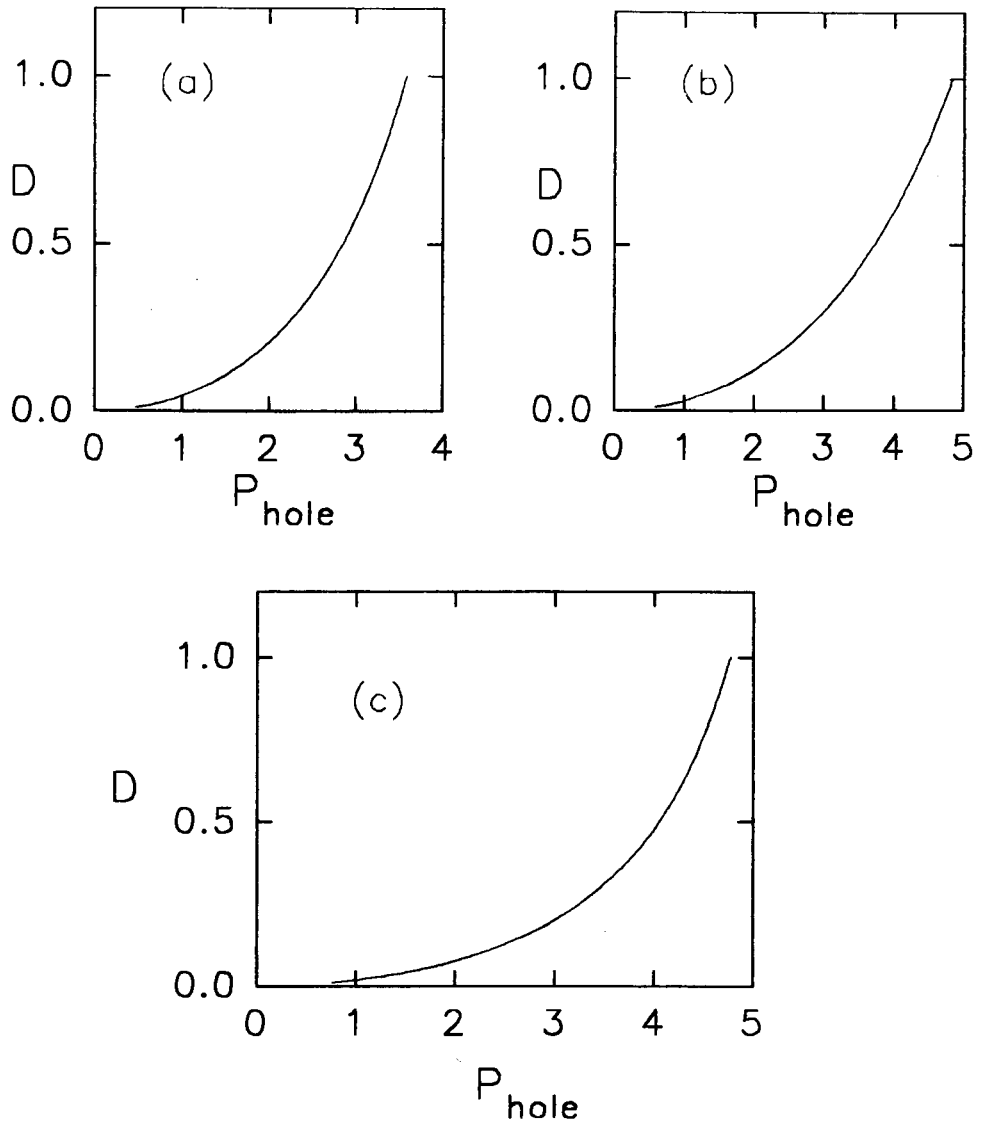

Figure 3.1: Modulation depth D vs. hole energy for dark solitons with $f = I - \alpha I^2$.
(a) - $I_{\max} = 5, \alpha = 0.5$
(b) - $I_{\max} = 2, \alpha = 0.5$
(c) - $I_{\max} = 8, \alpha = 0.1$

From this point there are several ways to seek bistability. Perhaps the most obvious approach is to look for dark solitons with the same background intensity ($I_{\max}$) and the same value of α, but different depths ($I_{\min}$). This would be more useful in practice than an approach which involves varying the background intensity, since, in experiment, dark solitons usually take the form of short holes in much broader bright pulses. Figure 3.2 shows the result of plotting $I_{\min}(\alpha)$ for several constant backgrounds in equation (3.35). $I_{\min}(\alpha)$ is single-valued, so in this sense the model $f = I - \alpha I^2$ does not support bistability.

Alternatively, the hole depth $I_{\min}$ can be held constant, and soliton solutions can be sought with the same α and different background intensities. The result of plotting $I_{\max}(\alpha)$ for various constant $I_{\min}$ is shown in Figure 3.3. $I_{\max}(\alpha)$ is double valued, so in this sense bistability can be said to exist for the model $f = I - \alpha I^2$. The inset in Figure 3.3 shows a pair of solitons for $\alpha \approx 0.0735$.

The definitions proposed above were developed independently from that of Gatz and Herrmann [34], who chose to hold the modulation depth $D = (I_{\max} - I_{\min})/I_{\max}$ constant . In terms of D, the transcendental equation is written:

$$(3 - 8\alpha I_{\max}) + (3 - 4\alpha(2 - D)\cosh\left(1.76\sqrt{\frac{\eta}{3}}\right) = \frac{4\eta}{I_{\max}D}, \qquad (3.36)$$

with $\eta = 3I_{\max}D(1 - \frac{2}{3}\alpha I_{\max}(4 - D))$. Plots of $I_{\max}$ vs. α for various constant values of D are shown in Figure 3.4. $I_{\max}$ is double valued in α, so in this sense, again, bistability can be said to exist. The inset in Figure 3.4 shows a pair of solitons for $\alpha \approx 0.086$ which are bistable by this definition.

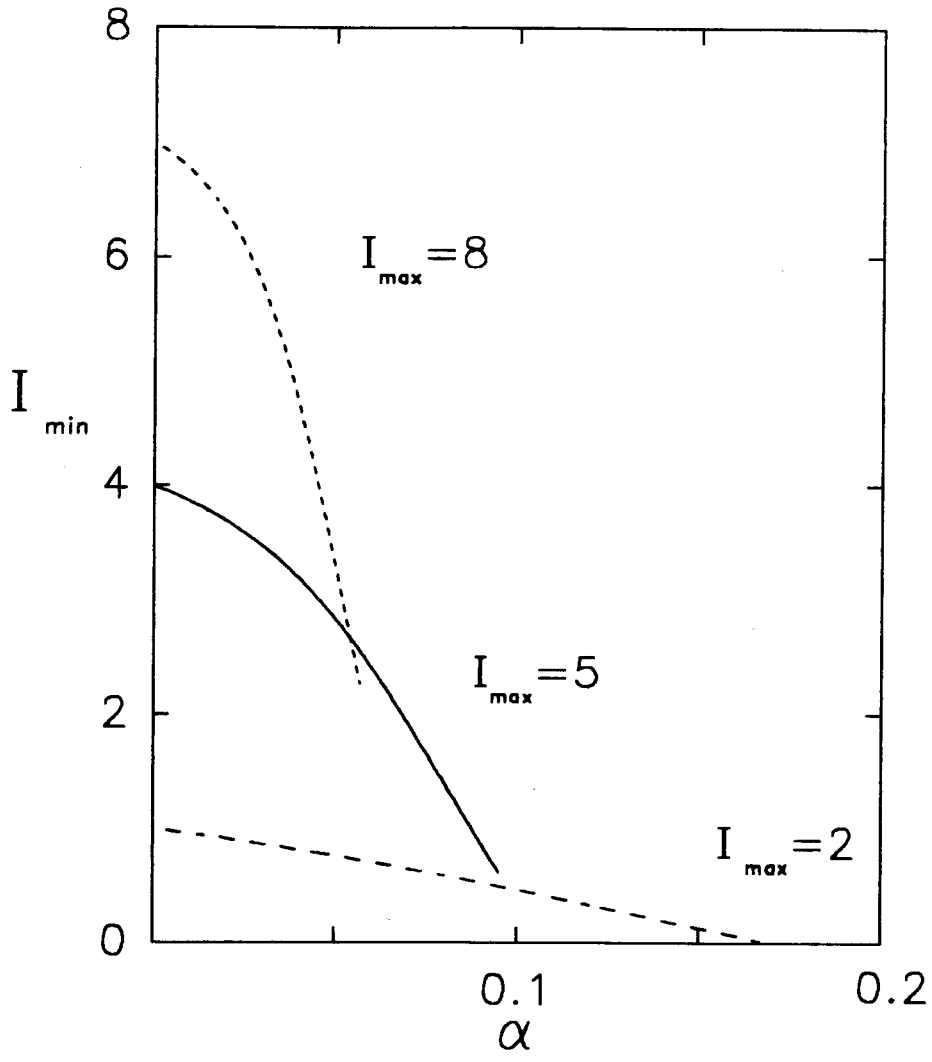

Figure 3.2: Depth $I_{\min}$ vs. parameter α for dark solitons with $f = I - \alpha I^2$. Curves for several different constant backgrounds $I_{\max}$ are shown.

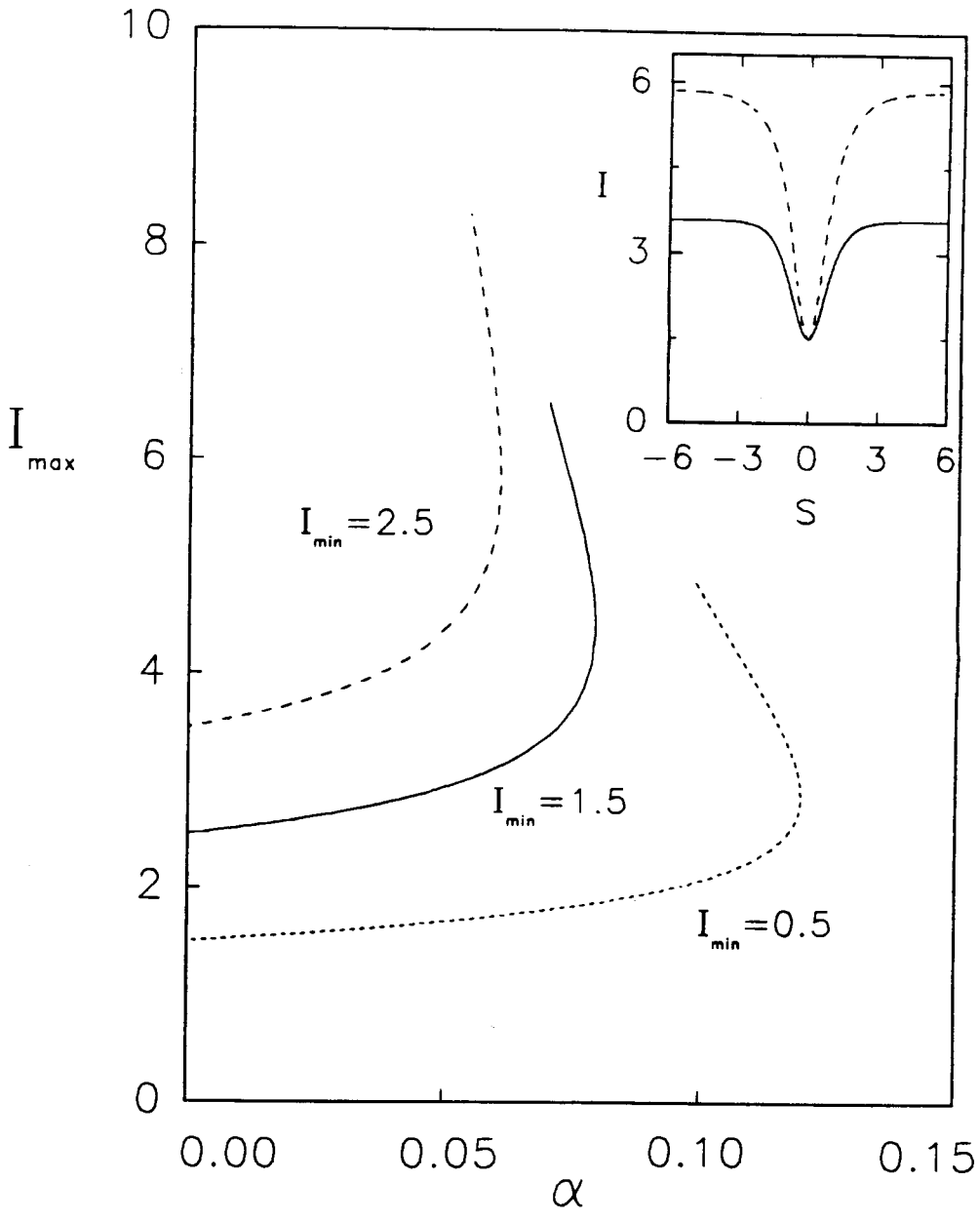

Figure 3.3: Background I_{max} vs. parameter α for dark solitons with $f = I - \alpha I^2$ and constant depth I_{min}. Curves for several different constant depths I_{min} are shown. (inset) - A pair of solitons with $\alpha \approx 0.0735$ and $I_{min} = 1.5$
dotted line - $I_{max} = 5.86$; solid line - $I_{max} = 3.58$

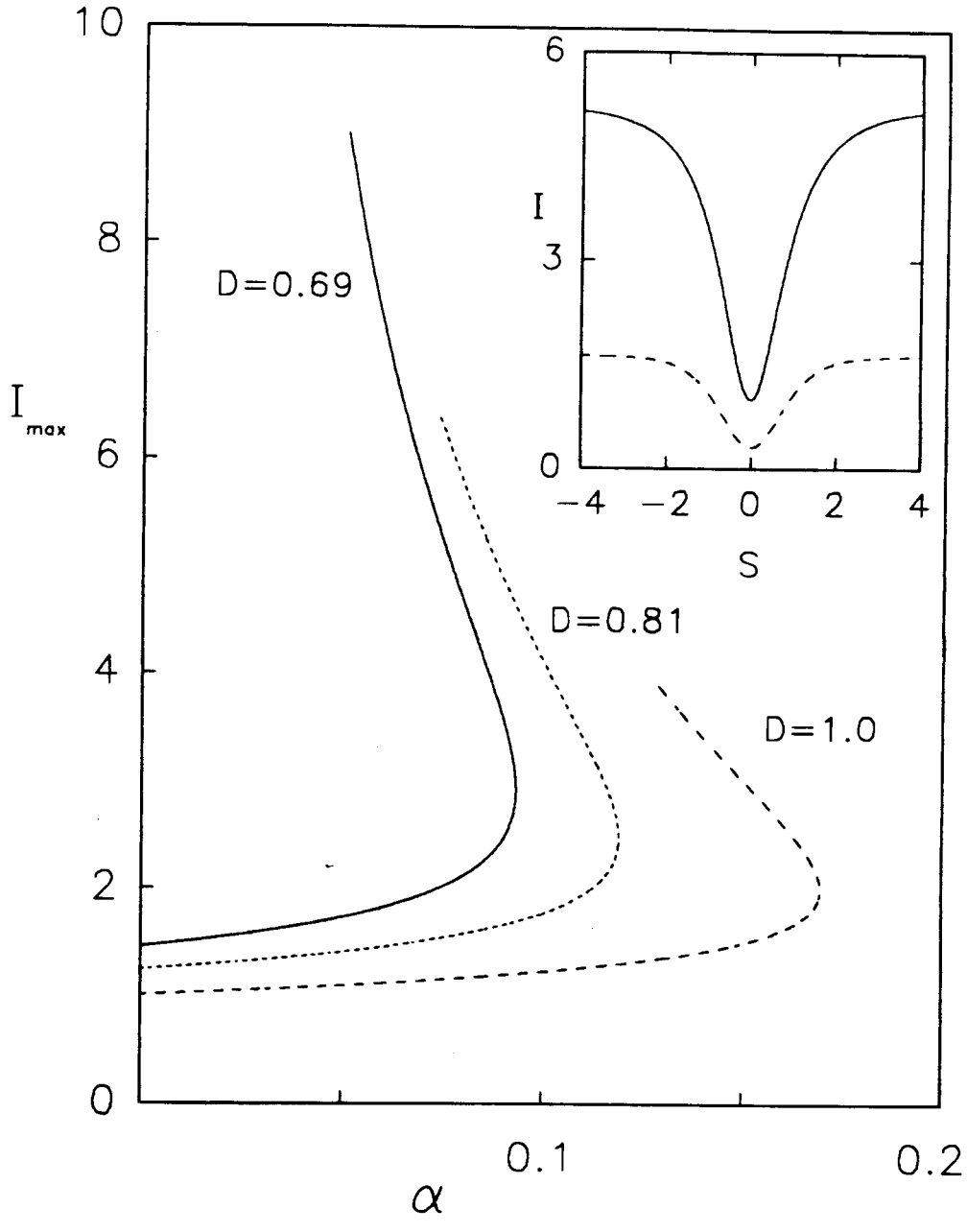

Figure 3.4: Background I_{max} vs. parameter α for dark solitons with $f = I - \alpha I^2$ and constant D. Curves for several different constant modulation depths D are shown. (inset) - A sample pair of solitons with $\alpha \approx 0.086$ and $D = 0.81$
solid line - $I_{max} = 5.21$; dotted line - $I_{max} = 1.62$

As yet, there is no standard definition for dark soliton bistability of the second kind. Of the possible definitions presented in this chapter, the second and third definitions provide bistability for the model $f = I - \alpha I^2$. However, it is not clear how these definitions would be put into practice experimentally, where the background intensity cannot be changed rapidly. The first definition presented here does not provide bistability for the model $f = I - \alpha I^2$, but is a better candidate for a standard definition because it would be convenient in experimental situations.

Chapter 4

Soliton Amplification

4.1 Theoretical Analysis

The generalized nonlinear Schrödinger equation can be solved exactly in many cases. This was shown in Chapter 2, where the GNLSE with anomalous dispersion and the nonlinearities given by equations (2.11) and (2.12) was solved to yield bright soliton solutions, and in Chapter 3, where the GNLSE with normal dispersion and the nonlinearity (2.11) was solved for dark soliton solutions. The variational method which is discussed in this section provides a way to find an approximate solution to the GNLSE, and is obviously useful when no exact solution can be found. Variational analysis is also useful in cases where an exact solution is known, as it can be used to describe the dynamics of pulses whose parameters do not lie exactly on the soliton line. Such pulses occur when solitons are amplified by multiplying their amplitudes by real constants, which is the simplest way to attempt switching.

Anderson [35] used the variational method to obtain an approximate solution of the NLSE with a Kerr nonlinearity ($f \propto |U|^2$). Here, a similar technique is used to

solve the GNLSE with anomalous dispersion (2.1).

The variational method is based on principles of Lagrangian dynamics. According to the principle of least action, equations of motion (also called variational equations) for a system are found by setting

$$\delta \int L(x_i, \frac{dx_i}{dt}, t)\, dt = 0\,, \tag{4.1}$$

where the *Lagrangian* , L, is formed by subtracting the system's total potential energy from its total kinetic energy. The quantities x_i are generalized position coordinates, and t is an independent variable of the system (time, for example). From equation (4.1), Lagrange's equations of motion can be derived:

$$\frac{\delta L}{\delta x_i} = \frac{d}{dt}\left(\frac{\partial L}{\partial\left(\frac{dx_i}{dt}\right)}\right) - \frac{\partial L}{\partial x_i} = 0 \tag{4.2}$$

and solved simultaneously to obtain the relationship between the position coordinates, their respective "velocities", dx_i/dt, and the independent variable t.

The GNLSE can be thought of as an "equation of motion" corresponding to the Lagrangian given by :

$$L = \frac{i}{2}\left(U\frac{\partial U^*}{\partial \xi} - U^*\frac{\partial U}{\partial \xi}\right) + \frac{1}{2}\left|\frac{\partial U}{\partial s}\right|^2 - F(|U|^2)\,, \tag{4.3}$$

where

$$F(I \equiv |U|^2) = \int_0^I f(I')dI'\,, \tag{4.4}$$

was introduced in Chapter 2. In this case, there are two independent variables, ξ and s, and the variational principle is given by:

$$\delta \int\int L\left(U, U^*, \frac{\partial U}{\partial \xi}, \frac{\partial U^*}{\partial \xi}, \frac{\partial U}{\partial s}, \frac{\partial U^*}{\partial s}\right) ds\, d\xi = 0\,. \tag{4.5}$$

The GNLSE is equivalent to:

$$\frac{\delta L}{\delta U^*} = \frac{\partial}{\partial \xi}\frac{\partial L}{\partial\left(\frac{\partial U^*}{\partial \xi}\right)} + \frac{\partial}{\partial s}\frac{\partial L}{\partial\left(\frac{\partial U^*}{\partial s}\right)} - \frac{\partial L}{\partial U^*} = 0\,. \tag{4.6}$$

In the variational method, a trial function is adopted to approximate U. The trial function depends on certain parameters, so that, when it is inserted into the variational principle, the result is a set of differential equations in the parameters. These differential equations can be solved simultaneously to give an approximate solution to the GNLSE, and can also give insight into the dynamics of pulse propagation.

Following Anderson, the trial wavefunction is chosen to have the form

$$U(\xi, s) = A(\xi)\,\mathrm{sech}\left(\frac{s}{a(\xi)}\right)\exp\left(ib(\xi)s^2\right) \tag{4.7}$$

where the pulse amplitude, A, is complex and a, b are real. a represents the pulse width and a non-zero b corresponds to the pulse developing a chirp (a frequency change over the pulse width).

Since the s-dependence in the trial wavefunction is explicit, one can integrate over s in equation (4.5) to obtain a reduced variational principle

$$\delta \int \langle L\rangle d\xi = 0 \tag{4.8}$$

with the reduced Lagrangian

$$\begin{aligned}\langle L\rangle &= \int_{-\infty}^{\infty} L ds \\ &= \frac{i}{2}\left(A\frac{dA^*}{d\xi} - A^*\frac{dA}{d\xi}\right) a\mathcal{J}_{10} \\ &\quad + |A|^2 a^3\left(\frac{db}{d\xi} + 2b^2\right)\mathcal{J}_{12} + \frac{1}{2}\frac{|A|^2}{a}\mathcal{J}_{30}\end{aligned}$$

$$-a\int_{-\infty}^{\infty} F(|A|^2\mathrm{sech}^2 x)dx\ . \tag{4.9}$$

It should be noted here that $x = s/a$ is a dummy variable of integration. In equation (4.9), the $\mathcal{J}$'s are integrals defined as follows:

$$\begin{aligned}
\mathcal{J}_{1m} &= \int_{-\infty}^{\infty} x^m \mathrm{sech}^2 x\, dx \\
\mathcal{J}_{2m} &= \int_{-\infty}^{\infty} x^m \mathrm{sech}^4 x\, dx \\
\mathcal{J}_{3m} &= \mathcal{J}_{1m} - \mathcal{J}_{2m} \\
\mathcal{J}_{4m} &= \int_{-\infty}^{\infty} x^m \mathrm{sech}^6 x\, dx
\end{aligned} \tag{4.10}$$

With the reduced Lagrangian, equation (4.2) can be used to create four variational equations:

$$\begin{aligned}
&\frac{\delta\langle L\rangle}{\delta A^*} = \frac{\partial}{\partial\xi}\left(\frac{\partial\langle L\rangle}{\partial\left(\frac{\partial A^*}{\partial\xi}\right)}\right) - \frac{\partial\langle L\rangle}{\partial A^*} = 0 \\
&\frac{\delta\langle L\rangle}{\delta A} = 0\ ,\quad \frac{\delta\langle L\rangle}{\delta a} = 0\ ,\quad \frac{\delta\langle L\rangle}{\delta b} = 0\ .
\end{aligned} \tag{4.11}$$

Upon substitution of equation (4.9) for $\langle L\rangle$, $\delta\langle L\rangle/\delta A^* = 0$ becomes

$$\begin{aligned}
\frac{d}{d\xi}\left(\frac{i}{2}Aa\mathcal{J}_{10}\right) &= \frac{-i}{2}\frac{dA}{d\xi}a\mathcal{J}_{10} + Aa^3\left(\frac{db}{d\xi} + 2b^2\right)\mathcal{J}_{12} \\
&\quad + \frac{1}{2}\frac{A}{a}\mathcal{J}_{30} + a\int_{-\infty}^{\infty}\frac{\partial F(|A|^2\mathrm{sech}^2 x)}{\partial A^*}dx\ .
\end{aligned} \tag{4.12}$$

Similarly, $\delta\langle L\rangle/\delta A = 0$ becomes

$$\begin{aligned}
\frac{d}{d\xi}\left(\frac{-i}{2}A^*a\mathcal{J}_{10}\right) &= \frac{i}{2}\frac{dA^*}{d\xi}a\mathcal{J}_{10} + A^*a^3\left(\frac{db}{d\xi} + 2b^2\right)\mathcal{J}_{12} \\
&\quad + \frac{1}{2}\frac{A^*}{a}\mathcal{J}_{30} + a\int_{-\infty}^{\infty}\frac{\partial F}{\partial A^*}dx\ ,
\end{aligned} \tag{4.13}$$

$\delta\langle L\rangle/\delta a = 0$ becomes

$$\frac{i}{2}\left(A\frac{dA^*}{d\xi} - A^*\frac{dA}{d\xi}\right)\mathcal{J}_{10} + 3|A|^2a^2\left(\frac{db}{d\xi} + 2b^2\right)\mathcal{J}_{12} - \frac{1}{2}\frac{|A|^2}{a^2}\mathcal{J}_{30} - \int_{-\infty}^{\infty} F dx = 0\,; \tag{4.14}$$

and $\delta\langle L\rangle/\delta b = 0$ becomes

$$\frac{d}{d\xi}(a^3|A|^2) = 4b|A|^2a^3\,. \tag{4.15}$$

This system of equations can be solved simultaneously to give $|A|^2a = C_0$, a constant of motion; $b = \frac{1}{2a}\frac{da}{d\xi}$; and also

$$\frac{d^2a}{d\xi^2} = \frac{\mathcal{J}_{30}}{\mathcal{J}_{12}a^3} + \frac{1}{\mathcal{J}_{12}|A|^2a}\int_{-\infty}^{\infty}[F(I) - If(I)]dx\,, \tag{4.16}$$

where $I = |A|^2\mathrm{sech}^2x$. Specific forms of $f(I)$ may be substituted at this point.

With the assumptions $a(\xi = 0) = a_0$ and $\left.\frac{da(\xi)}{d\xi}\right|_{\xi=0} = 0$, equation (4.16) becomes

$$\frac{1}{2}\left(\frac{dy}{d\xi}\right)^2 + \Pi(y) = 0, \tag{4.17}$$

where $y = a/a_0$.

For the model $f = I - \alpha I^2$, $\Pi(y)$ is given by

$$\Pi(y) = \frac{\overline{\mu}}{y^2} + \frac{\nu}{y} - (\overline{\mu} + \nu) \tag{4.18}$$

where

$$\begin{aligned}\overline{\mu} &= \frac{\mathcal{J}_{30}}{2\mathcal{J}_{12}a_0^4} + \frac{1}{3}\frac{\alpha\mathcal{J}_{40}|A_0|^4}{\mathcal{J}_{12}a_0^2}\\ \nu &= \frac{-\mathcal{J}_{20}|A_0|^2}{2\mathcal{J}_{12}a_0^2}\,.\end{aligned} \tag{4.19}$$

Equation (4.17) is analogous to the equation of motion for a particle starting from rest at $y = 1$ in a potential well, with the potential $\Pi(y)$ given by equation (4.18). Equation (4.18) has the same form as the "potential well" equation developed by Anderson [35]. Anderson's μ has been renormalized in (4.19) into $\overline{\mu}$ to take the contribution of nonzero α into account.

Anderson identified the following properties of $\Pi(y)$:

$$\Pi(y) \rightarrow \begin{cases} \infty & y \rightarrow 0 \\ -(\overline{\mu}+\nu) & y \rightarrow \infty \end{cases},$$

$$\Pi(y) = 0 \text{ for } y = 1 \text{ and } y = -(1+\nu/\overline{\mu})^{-1} \equiv y_0 ,$$

$$\Pi'(y) = 0 \text{ for } y = y_m = -2\overline{\mu}/\nu ,$$

$$\Pi'(1) = -\overline{\mu}(2+\nu/\overline{\mu}) ,$$

$$\Pi(y_m) = -(2\overline{\mu}+\nu)^2/(4\overline{\mu}) \leq 0 .$$

For distinct ranges of the value of $\nu/\overline{\mu}$, and hence for distinct regions of α/A_0 space, the qualitative behaviour of a pulse can be predicted based on the shape of $\Pi(y)$.

When $(-1 < \nu/\overline{\mu} < 0)$, the minimum of the potential is at $y > 1$, and the potential has only one zero since $-(\overline{\mu}+\nu) < 0$ (See Figure 4-1). Starting at 1, y will increase indefinitely, since the potential well is not deep enough to prevent the increase. Physically, this means that the nonlinearity opposes pulse spreading, but is not strong enough to overcome it. The pulse broadens and disperses.

When $(-2 < \nu/\overline{\mu} < -1)$, the minimum of the potential is at $y > 1$, and there is a potential well between $y = 1$ and $y = y_0 = -(1+\nu/\overline{\mu})^{-1}$ (see Figure 4-2). The mechanical analogy suggests that y, starting from 1, will oscillate between the zeros

of $\Pi(y)$. Physically, this means that the nonlinearity stops the initial broadening, causing the pulse to oscillate after first becoming broader. The oscillation of the pulse width is expected to be accompanied by an oscillation in height, since $|A|^2 a = C_0$ is a constant of motion.

When $(\nu/\overline{\mu} < -2)$, the minimum of the potential is at $y < 1$, and a potential well exists between $y = 1$ and $y = y_0 = -(1 + \nu/\overline{\mu})^{-1}$ (see Figure 4-3). In this case, the physical interpretation is that nonlinear effects dominate initially but are countered by dispersion. The pulse oscillates after first becoming narrower.

When $\nu/\overline{\mu} = -2$, $y_0 = y_m = 1$. The potential well collapses into a single point, and, if y starts at this point, it will not change. This situation corresponds to a balance between the nonlinear and dispersive effects which allows the pulse to propagate unchanged. In other words, the pulse is a bright soliton solution. The line in α / A_0 space defined implicitly by $\nu/\overline{\mu} = -2$ is an approximation to the soliton line given by equation (2.20) .

The boundary lines $\nu/\overline{\mu} = -1$ and $\nu/\overline{\mu} = -2$ are shown in Figure 4-4, along with the exact solution. Since the line $\nu/\overline{\mu} = -2$ is only a rough approximation to the soliton line, it can be expected that the line $\nu/\overline{\mu} = -1$ is also only an approximate boundary. This suggests that input pulses for which α and A_0 lie very close to the boundaries of the above regions may not behave exactly as predicted.

Evaluating the relevant integrals in equation (4.19), we have

$$\frac{\nu}{\overline{\mu}} = -\frac{2A_0^2 a_0^2}{1 + \frac{16}{15}\alpha A_0^4 a_0^2} \tag{4.20}$$

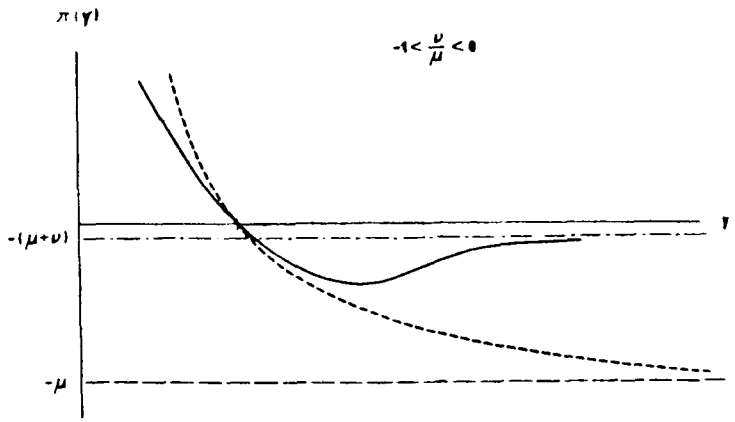

Figure 4.1: Qualitative plot of $\Pi(y)$ for $(-1 < \nu/\overline{\mu} < 0)$ from Anderson. The case of linear dispersion is given for comparison (- - -)

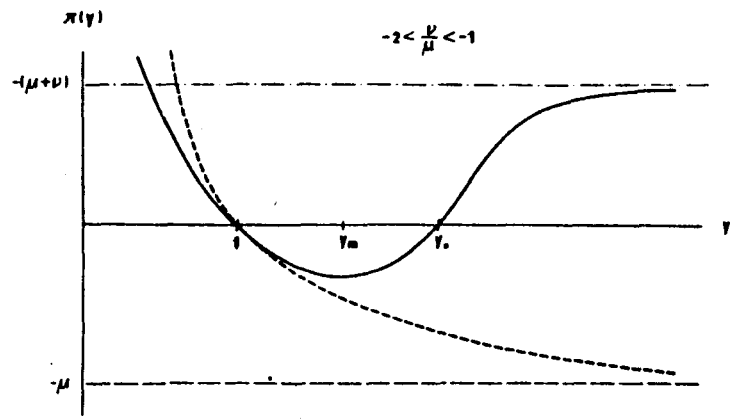

Figure 4.2: Qualitative plot of $\Pi(y)$ for $(-2 < \nu/\overline{\mu} < -1)$ from Anderson. The case of linear dispersion is given for comparison (- - -)

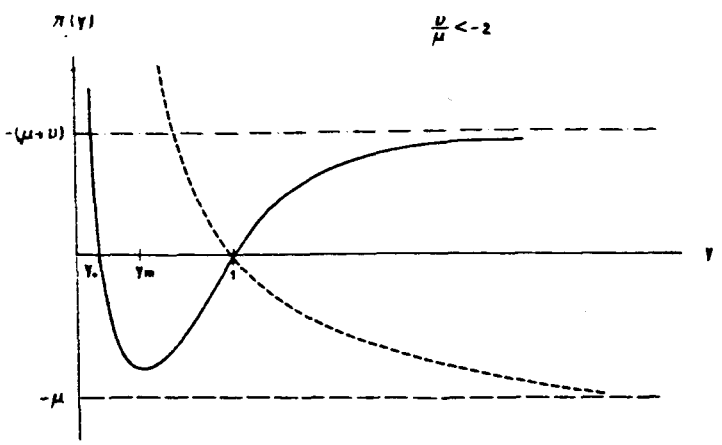

Figure 4.3: Qualitative plot of $\Pi(y)$ for $(\nu/\overline{\mu} < -2)$ from Anderson. The case of linear dispersion is given for comparison (- - -)

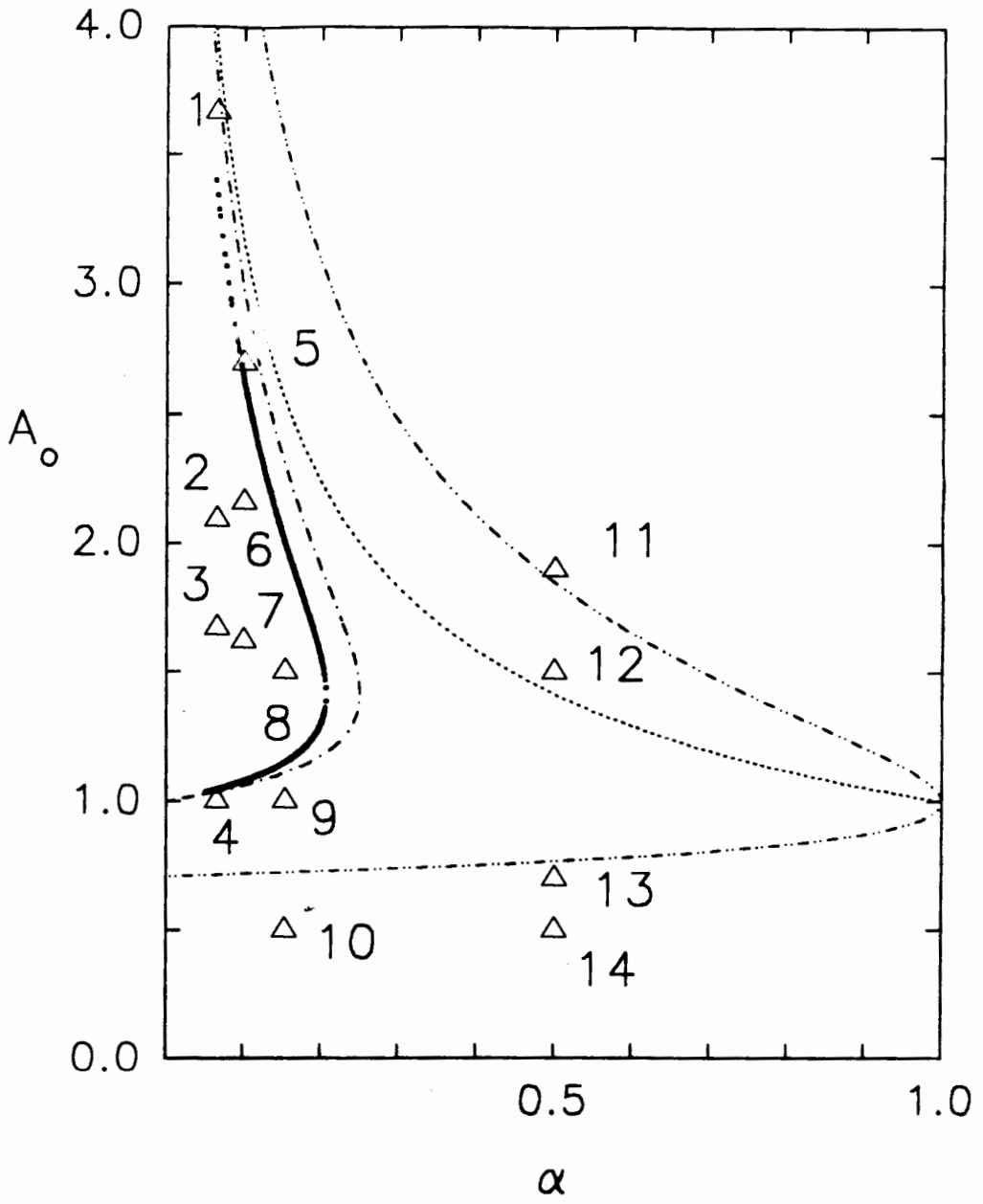

Figure 4.4: Amplitude vs. parameter α for $f = I - \alpha I^2$ with amplified input pulses shown.

solid line - soliton line given by (2.20)

- - - $\alpha I = 1$

$- \cdot - \nu/\overline{\mu} = -2$

$- \cdot \cdot - \nu/\overline{\mu} = -1$

$\triangle$ - experimental input amplified pulses (KA_0 in Table 4-1).

When $\alpha \neq 0$, $\nu/\overline{\mu}$ given by equation (4.20) increases for A_0 increasing from zero, but will eventually begin to decrease. For the Kerr model studied by Anderson [35], $\alpha = 0$, so that $\nu/\overline{\mu}$ increases monotonically with increasing input intensity. The more complex dependence of $\nu/\overline{\mu}$ on A_0 allows bistability to be possible, since the line in α / A_0 space defined by $\nu/\overline{\mu} = -2$ bends back on itself. Moreover, more complex pulse behaviour is possible for the model $f = I - \alpha I^2$, since, for example, dispersive effects dominate at both large and small amplitudes for many values of α.

It should be noted that the dimensionless soliton units were chosen to normalize the pulse intensity FWHM to that of $\mathrm{sech}^2(s)$. In these units, the width parameter $a_0 = 1$.

The dotted line in Figure 4-4 represents $\alpha I = 1$. For initial amplitudes (A_0) above this line, the function f is negative, and the nonlinearity changes sign. We can expect solitons with parameters α and A_0 lying above the dotted line to behave in an unusual manner, since parts of their amplitudes will be subjected to a positive nonlinearity and parts to a negative nonlinearity.

For the saturable nonlinearity (2.12), it is possible to carry out an analysis similar to that above, using the considerably more complex $\Pi(y)$:

$$\begin{aligned}\Pi(y) &= \frac{\mathcal{J}_{30}}{2\mathcal{J}_{12}a_0^4}\left(\frac{1}{y^2}-1\right) \\ &+\frac{1}{\mathcal{J}_{12}\gamma a_0^2\sqrt{\gamma|A_0|^2}}\left[\frac{y}{\sqrt{y+\gamma|A_0|^2}}\tanh^{-1}\sqrt{\frac{\gamma|A_0|^2}{y+\gamma|A_0|^2}}\right. \\ &\left.-\frac{1}{\sqrt{1+\gamma|A_0|^2}}\tanh^{-1}\sqrt{\frac{\gamma|A_0|^2}{1+\gamma|A_0|^2}}\right]\end{aligned} \tag{4.21}$$

Such a detailed analysis is not included here. By setting $(d\Pi/dy)_{y=1} = 0$ (this is analogous to setting $y_0 = y_m = 1$ in the previous model) and $a_0 = 1$ (to account for soliton units), the variational approximation to the exact soliton curve (2.23) is found to be:

$$1 + \frac{4}{3}\gamma(1 + \gamma I_0) = \frac{(1 + 2\gamma I_0)}{\sqrt{\gamma I_0(1 + \gamma I_0)}} \tanh^{-1} \sqrt{\frac{\gamma I_0}{1 + \gamma I_0}} \tag{4.22}$$

with $I_0 = |A_0|^2$. Equation (4.22) is shown in Figure 4-5 for comparison with the exact soliton line (2.23).

4.2 Numerical Amplification

The predictions of the variational method for $f = I - \alpha I^2$ can be compared to the numerical behaviour of amplified solitons. For the following numerical experiments, the explicit three-step scheme, described in Chapter 2, was used again. An input pulse was formed for each experiment by choosing a point from the soliton line (2.20), and using the chosen α and A_0 in equation (2.17). The resulting amplitude function is multiplied by an amplification factor K to give a pulse of the form:

$$U(s, \xi = 0) = K\sqrt{I(s)} \tag{4.23}$$

The initial α and A_0 values, and the amplification constants, are shown in Table 4-1 along with the observed result of each numerical experiment.

The numbered triangles in Figure 4-4 correspond to the pairs of α and KA_0 values for the input pulses described in Table 4-1. Figures 4-6 - 4-9 show some representative numerical runs.

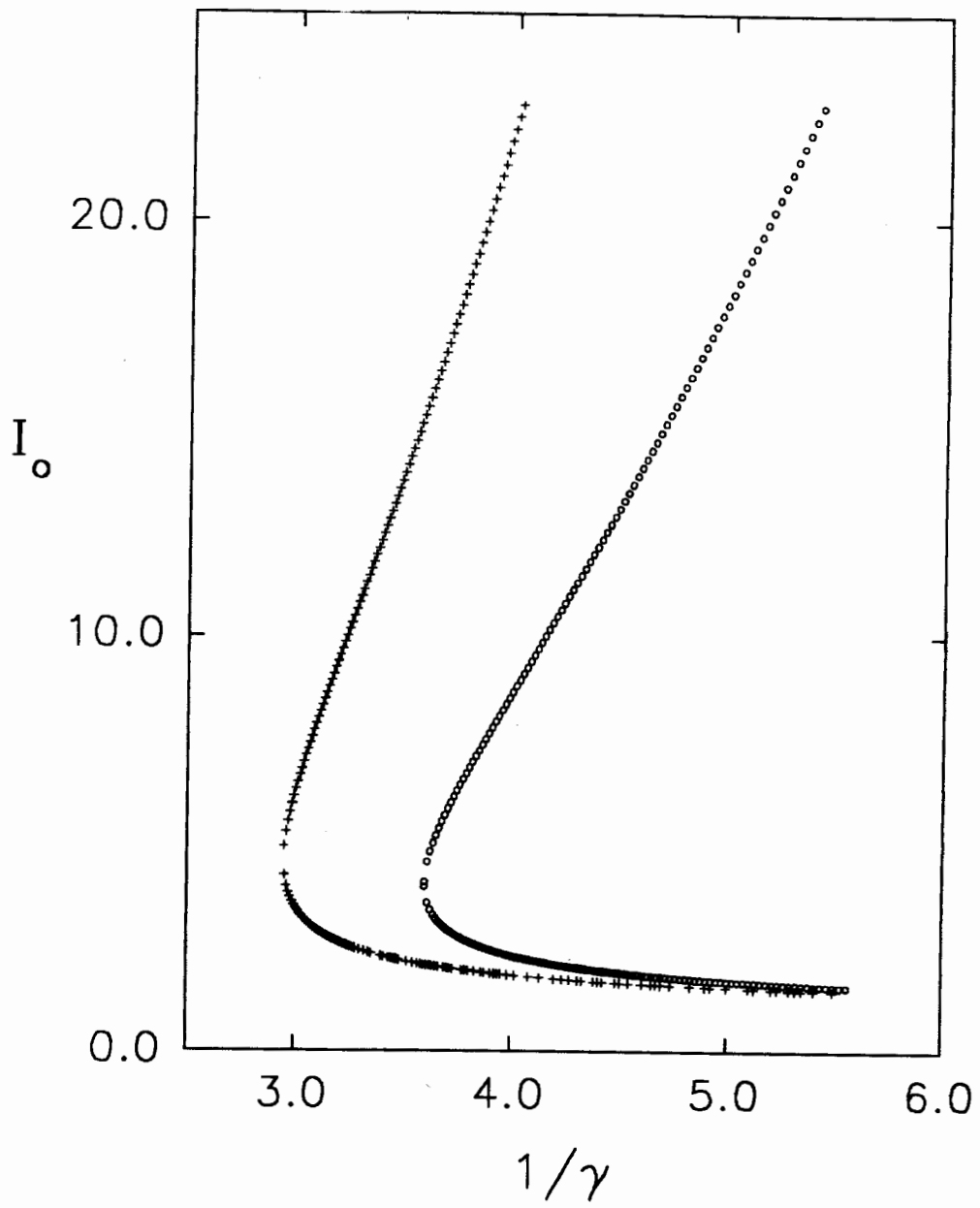

Figure 4.5: Intensity I_0 vs. parameter γ^{-1} for the saturable model with variational approximation shown

$\cdots$ (right-hand line) - exact soliton line given by equation 2.23

+++ (left-hand line)- approximate soliton line given by equation 4.22

Table 4.1: Some representative results of amplification experiments for the model $f = I - \alpha I^2$. See also Figure 4-4.

	α	A_0	K	$\nu/\overline{\mu}$	Numerical result
1	0.065	1.047	3.5	-1.99	narrows, then disintegrates
2	0.065	1.047	2.0	-2.33	narrows and oscillates
3	0.065	3.344	0.5	-3.63	narrows and osc., then switches
4	0.065	3.344	0.3	-1.88	broadens and oscillates
5	0.10	1.080	2.5	-2.19	narrows, then disintegrates
6	0.10	1.080	2.0	-2.81	narrows and osc., then switches
7	0.10	1.080	1.5	-3.03	narrows and oscillates
8	0.153	2.005	0.75	-2.47	narrows and osc., then switches
9	0.153	2.005	0.5	-1.73	broadens and oscillates
10	0.153	2.005	0.25	-0.50	disperses
11	0.50	1.0	1.9	-0.91	disperses, then splits
12	0.50	1.0	1.5	-1.22	broadens and oscillates
13	0.50	1.0	0.7	-0.86	broadens and oscillates
14	0.50	1.0	0.5	-0.48	disperses

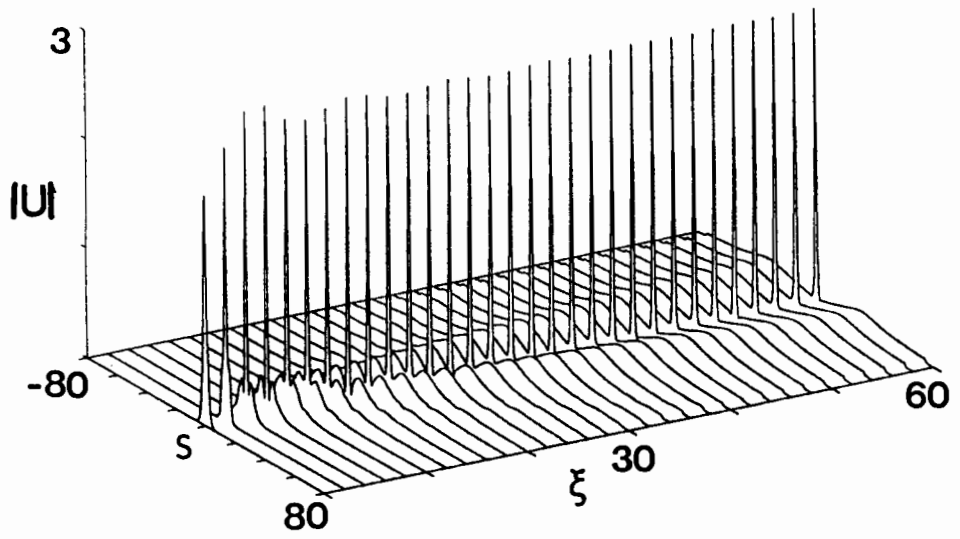

Figure 4.6: Amplification run 2 (refer to Figure 4-4 and Table 4-1), showing an inital narrowing and oscillation. A is the pulse amplitude.

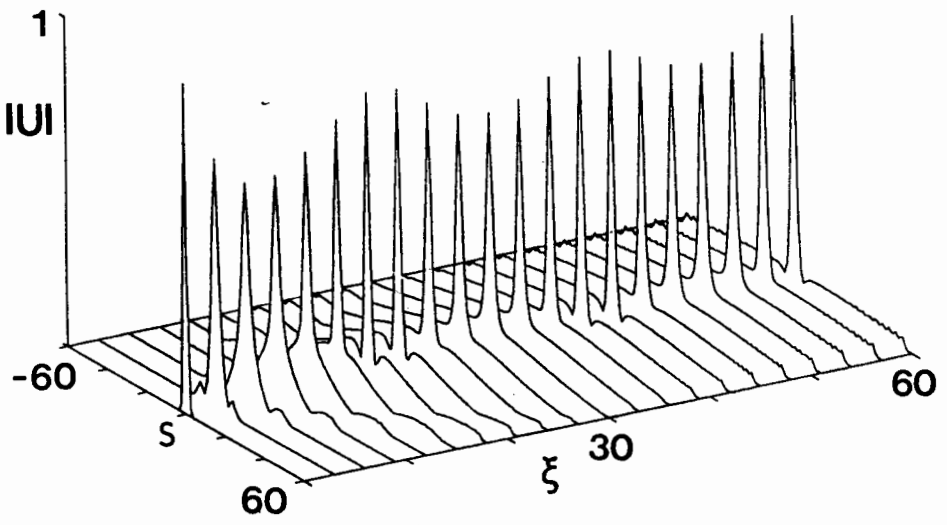

Figure 4.7: Amplification run 4, showing an initial broadening and oscillation.

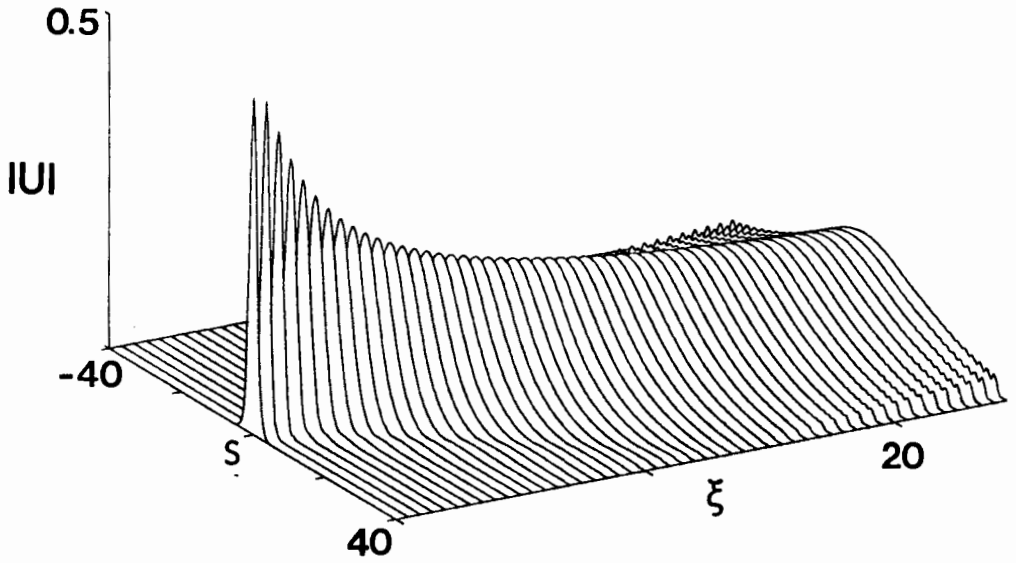

Figure 4.8: Amplification run 10, showing dispersion.

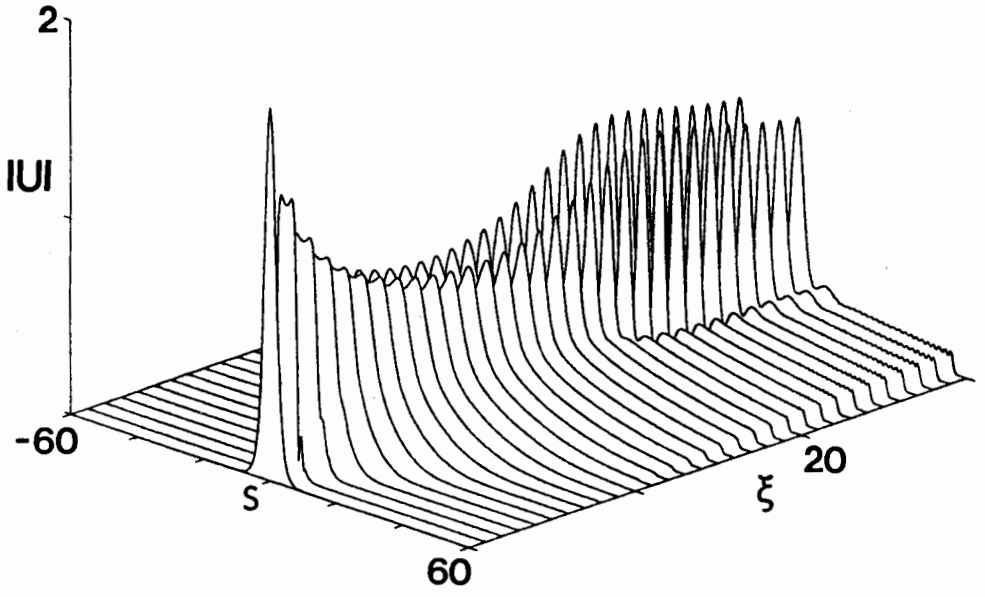

Figure 4.9: Amplification run 11, showing dispersion and splitting of the pulse.

The numerical results shown in Table 4-1 agree with the predictions based on analysis of $\nu/\overline{\mu}$ which are summarized in Figure 4-4 . In experiments 1 and 5, the pulse degenerates into a large number of sharp spikes. The input soliton for each of these cases lies near the line $\alpha I = 1$, and the initial upward oscillations put the peak value above this line. For I above this line, the function f becomes negative. The pulse may disintegrate because parts of it are subjected to a negative nonlinearity, and parts to a positive nonlinearity. This disintegration also occurred in one of the collision runs in Chapter 2.

In experiment 11, the input pulse again extends above the line $\alpha I = 1$. The variational method correctly predicts the initial dispersion, but does not account for the splitting (see Figure 4-9). The pulse in experiment 13 broadens and oscillates, although the variational method predicts dispersion. The input pulse for experiment 13 lies very close to the line $\nu/\overline{\mu} = -1$. Since the $\nu/\overline{\mu}$ lines can give only a rough indication of the regions where different behaviour is expected, the variational approximation fails to accurately predict its behaviour.

The results in Table 4-1, when compared to the predictions summarized in Figure 4-4 indicate that the variational analysis is a helpful tool for predicting the general behaviour of pulses whose initial α and A_0 values do not lie too close to the boundary lines $\nu/\overline{\mu} = -2$ and $\nu/\overline{\mu} = -1$ or to the line $\alpha I = 1$. The variational method is not able to predict the switches which are observed numerically (in experiments 3, 6, and 8, for example). This is because its predictions are based on the assumption that

the pulse shape does not undergo any radical or permanent change. In runs where switching takes place, the pulse shape typically *does* change as some radiation is shed in the form of side pulses. Switching is discussed in more detail in Chapter 5, for both the model described by $f = I - \alpha I^2$, and the model described by equation (2.12). Both the variational analysis and the numerical amplification studies described here are included in a paper which has recently been accepted for publication in Physical Review [2].

Chapter 5

Switching

As was discussed in Chapter 1, bistable solitons provide a way of coding binary information which makes switching possible between the ones (represented by high-state solitons) and the zeros (represented by low-state solitons). Ideally, the switching mechanism should be reversible, and the ones and zeros should be easily distinguishable.

Enns et al. (see [1] and references therein) have demonstrated switching between BISOL1 states for several models which yield N-shaped $P(\beta)$ curves. The high-state solitons on the upper positive slope branch can be easily distinguished from the low-state solitons on the lower positive-slope branch, since they are separated by a negative-slope unstable region. Upswitching from low to high states and downswitching from high to low states were carried out by amplification and by evanescent coupling.

In the amplification method, the input soliton was subjected to localized damping or a localized energy source, which had the effect of multiplying the pulse amplitude

by a constant. Upswitching was observed for some strengths of the energy source, and downswitching for some strengths of localized damping. It was found that back-and-forth switches without hysteresis were not generally possible between high and low states which are far from the unstable region [36].

The evanescent coupling procedure makes use of crosstalk between optically coupled fibers (again, see [1]). In this method, two or more fibers are coupled slightly over a limited distance. Downswitching has been observed when energy from a soliton introduced into one fiber leaks into one or more other, initially empty fibers. A form of upswitching, soliton fusion, has been observed when low state solitons are introduced into four outer fibers around an initially empty fiber. When appropriate parameters are chosen, a high-state soliton can be formed in the central fiber.

It is natural to ask next whether similar switching operations can be performed on BISOL2. In the collision experiments of Gatz and Herrmann [29], which were repeated in Chapter 2, there is evidence to suggest that a low-state soliton may be one of the results of a collision between two high-state solitons. These collisions were performed numerically using the model $f = I - \alpha I^2$. The amplification runs of Chapter 4 also use the model $f = I - \alpha I^2$, and there is evidence to suggest switching in runs 3, 6 and 8 (refer to Table 4.1). In this chapter, switching is investigated in more detail, for both the model described by $f = I - \alpha I^2$ and the saturable model described by equation (2.12).

The numerical scheme used here is the same explicit scheme used in Chapters 2

and 4. As in Chapter 4, the input pulse is formed by choosing pairs of parameters (α and A_0, or γ and I_0) from the soliton line and using them in either equation (2.17), for $f = I - \alpha I^2$, or equation (2.21), for the saturable model. The amplitude function is then multiplied by a factor K, where $K > 1$ for attempted upswitching and $K < 1$ for attempted downswitching.

For the model $f = I - \alpha I^2$, the output pulse was fit using the same method which was described in section 2.4. For the saturable model, it was necessary to modify the fitting routine slightly, since equation (2.21) for the form of the soliton can be solved explicitly for $s(I)$, but not for $I(s)$. The output pulse is fitted to the soliton line by varying I_0 in equation (2.21) for $s(I_i)$, which is evaluated at each I_i from the output pulse data. If the chosen I_0 is smaller than I_i, then equation (2.21) involves the square root of a negative quantity; the fitting routine ignores such points. The best fit I_0 is then chosen to be the one which minimizes the value of

$$\frac{\sum_i \left(s_{\text{expt}}(I_i) - s_{\text{fit}}(I_i)\right)^2}{\text{number of points fit}}, \tag{5.1}$$

where the $s_{\text{expt}}(I_i)$ come from the output pulse data. The results presented in this chapter are included in [2], which has been accepted for publication in Physical Review.

5.1 Switching for $f = I - \alpha I^2$

The results of some representative switching experiments for the model $f = I - \alpha I^2$ are summarized in Table 5.1 which shows the inital (subscript i) and final (subscript

f) scaled values of α and A_0 for each run, along with the amplification constant K.

Table 5.1: Some representative switching results for the model $f = I - \alpha I^2$. Subscript i indicates inital values, f indicates final (scaled) values. K is the amplification factor. See also Figure 5.1.

	α_i	A_{0i}	K	α_f	A_{0f}
A	0.120	1.100	1.60	0.201	1.542
B	0.153	2.005	0.75	0.206	1.368
C	0.100	2.631	0.50	0.149	1.142
D	0.065	3.344	0.50	0.183	1.221
E	0.100	1.080	2.00	0.162	1.921
F	0.149	1.146	2.00	0.100	2.629

Figure 5.1 shows the soliton line with the initial and final pulses for each switch indicated. Both upswitching and downswitching were observed. In many cases, the difference in amplitude between the initial and final states was quite large.

Representative switching runs are shown in Figures 5.2 and 5.4. Corresponding fits of the output pulses are shown in Figures 5.3 and 5.5. It is clear from these excellent fits that switching has occurred.

For the BISOL2 supported by the nonlinearity $f = I - \alpha I^2$, back-and-forth switches with essentially no hysteresis appear to be possible between C_i and C_f, and between E_i and E_f (refer to Table 5.1 and Figure 5.1). In both cases, the upswitch was accomplished using an amplification factor of 2.0, and the downswitch using an amplification factor of 0.5. In the first case, the final A_0 after the upswitch is within 0.1% of the initial A_0 of the downswitch. In the second case, the final A_0 was within

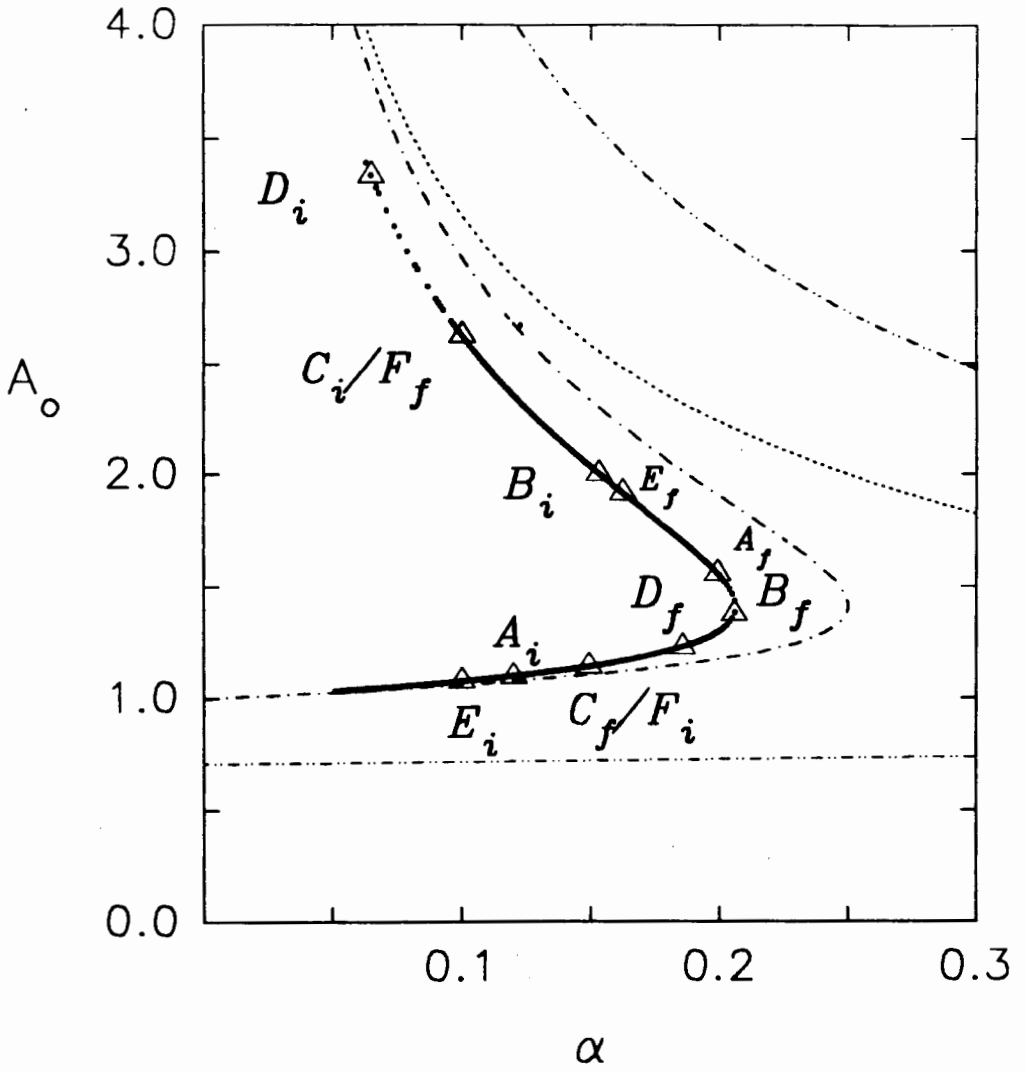

Figure 5.1: Amplitude vs. parameter α for $f = I - \alpha I^2$.
$\cdots$ - soliton line
$- - -$ $\alpha I = 1$
$- \cdot - \nu/\overline{\mu} = -1$
$- \cdot \cdot - \nu/\overline{\mu} = -2$
$\triangle$ - initial and final pulses from switching experiments (see Table 5.1).

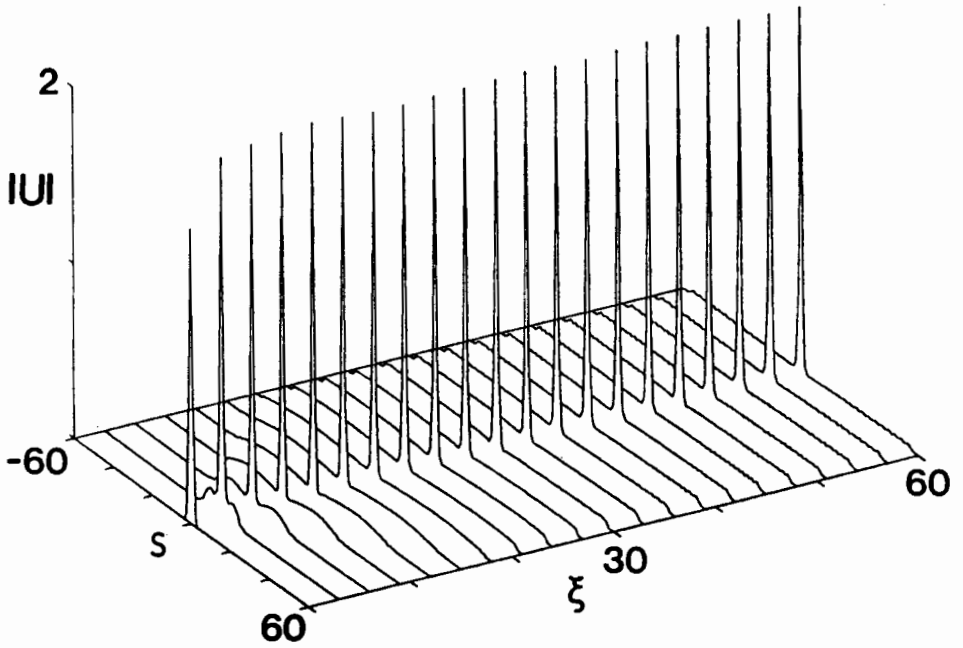

Figure 5.2: Downswitch from D_i to D_f (refer to Figure 5.1 and Table 5.1).

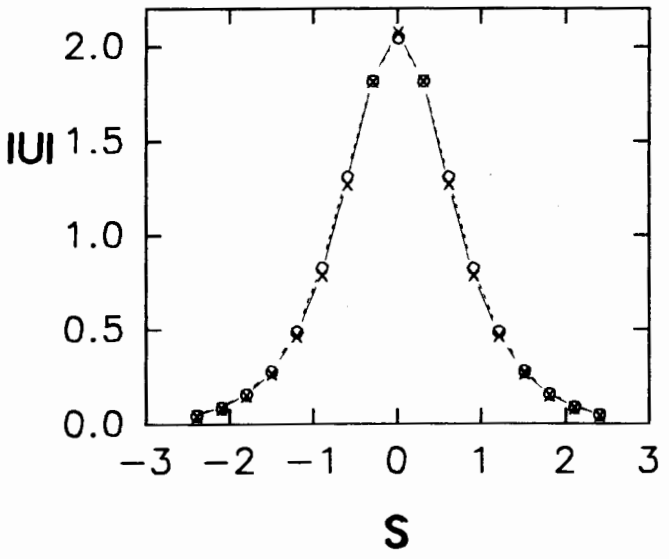

Figure 5.3: Least squares fit of the output pulse from downswitching run D.
x - numerical result
o - best fit soliton

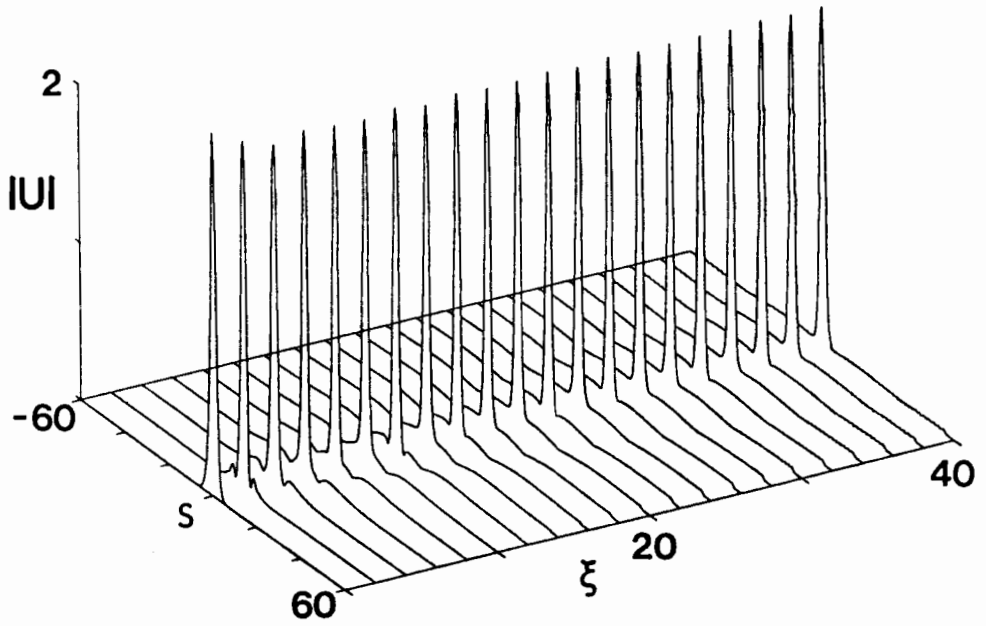

Figure 5.4: Upswitch from F_i to F_f (refer to Figure 5.1 and Table 5.1).

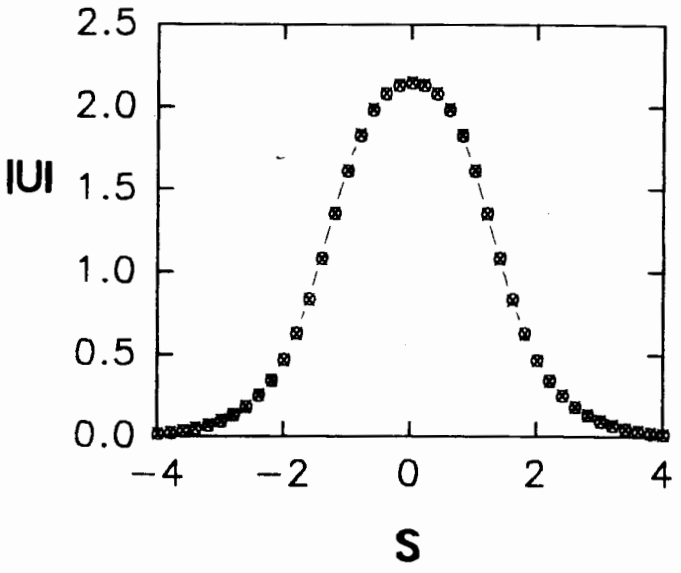

Figure 5.5: Least squares fit of the output pulse from upswitching run F.
x - numerical result
o - best fit soliton

2% of the initial A_0 of the downswitch.

5.2 Switching for the Saturable Model

Some representative results of switching experiments for the saturable model are shown in Figure 5.6 and described further in Table 5.2. Subscript i again indicates the initial pulse, while subscript f indicates the final (scaled) pulse. Again, both upswitching and downswitching are possible.

Table 5.2: Some representative switching results for the saturable model. Subscript i indicates initial values, f indicates final (scaled) values. K is the amplification factor. See also Figure 5.6.

	$(1/\gamma)_i$	I_{0i}	K	$(1/\gamma)_f$	I_{0i}
G	[illegible]	2.320	2.800	5.337	22.122
H	[illegible]	9.870	0.500	3.973	2.332
K	3.704	2.946	2.000	4.505	13.341
L	5.337	22.122	0.357	4.016	2.284
M	5.319	1.634	5.000	7.457	51.731

Representative switching runs are shown in Figures 5.7 and 5.9. The fits shown in Figures 5.8 and 5.10 are again very good, providing clear evidence for switching.

There is also evidence of an essentially hysteresis-free back-and-forth switch, between G_i and G_f.

For the saturable model, the nonlinearity $f(I)$ is always positive, so the difficulties that arose in Chapter 4 for the model $f = I - \alpha I^2$ when the amplitude of a pulse was above the line $\alpha I = 1$ do not exist here. For this reason, it is possible to switch

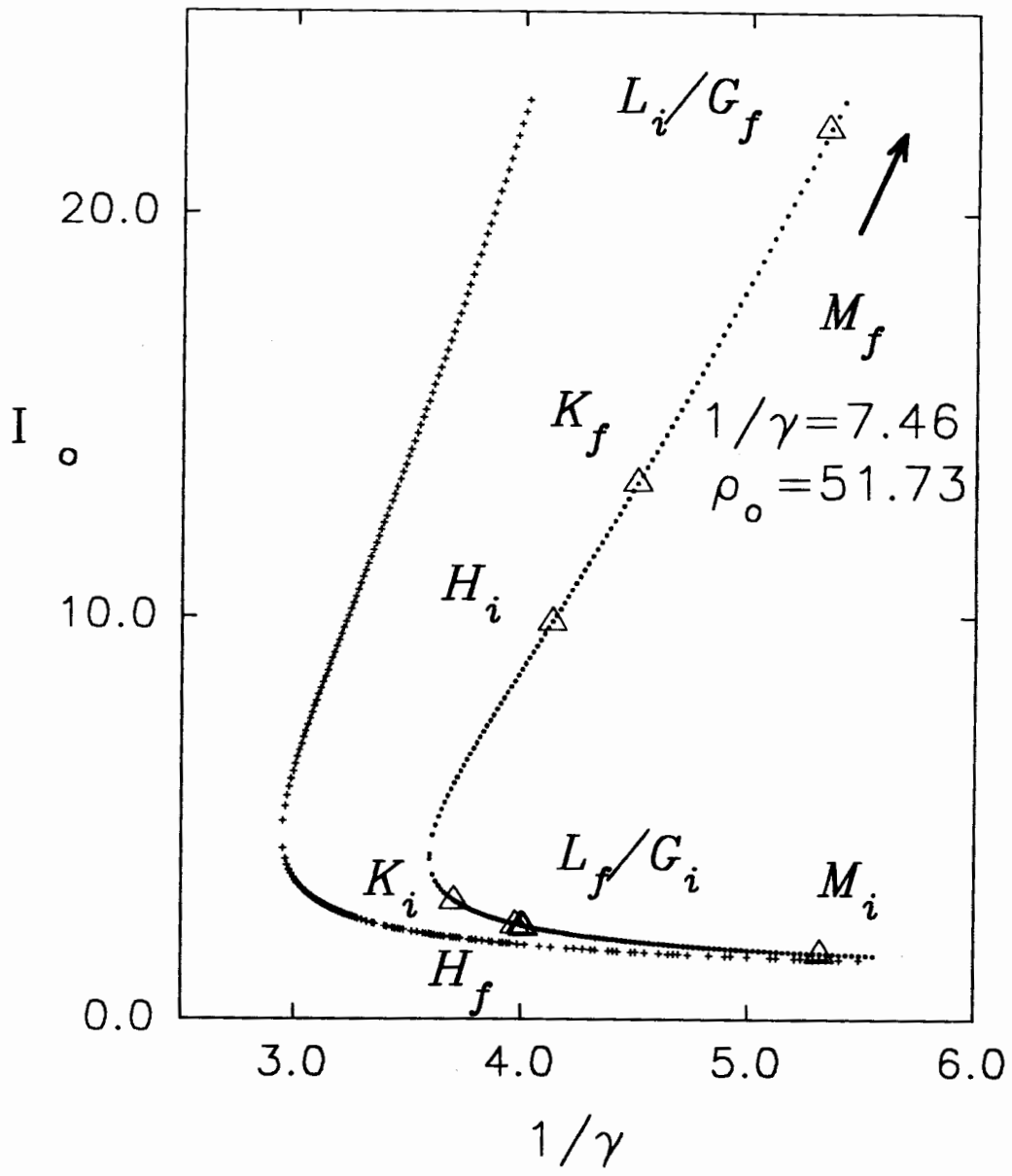

Figure 5.6: Intensity I_0 vs. parameter γ^{-1} for the saturable model.
$\cdots$ (right-hand line) - exact soliton line given by 2.23
+++ (left-hand line)- approximate soliton line given by 4.22
$\triangle$ - initial and final pulses from switching experiments (see Table 5.2).

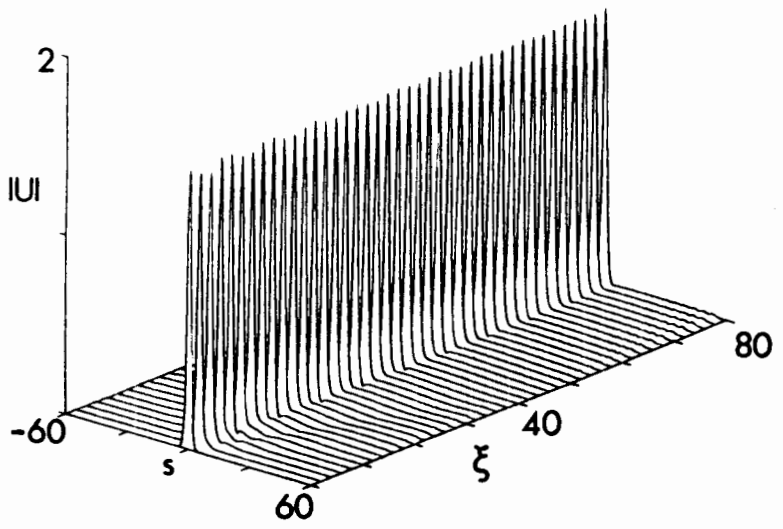

Figure 5.7: Downswitch from H_i to H_f (refer to Figure 5.6 and Table 5.2).

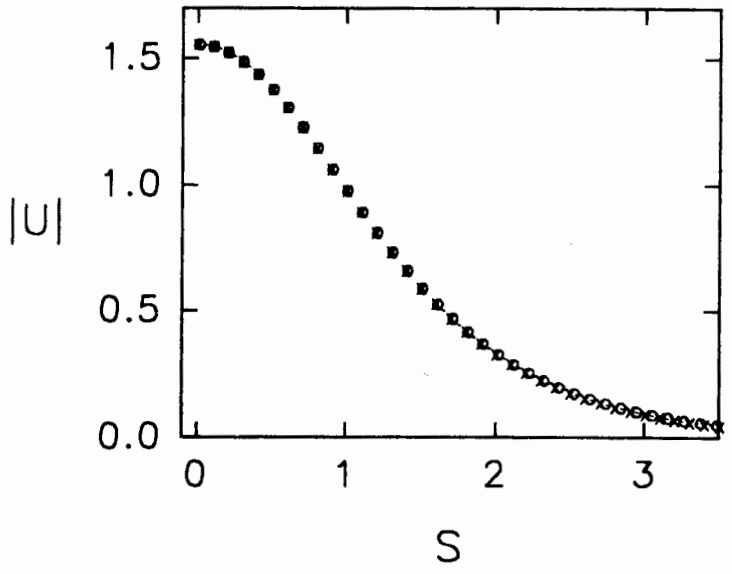

Figure 5.8: Least squares fit of the output pulse from downswitching run H.
x - numerical result
o - best fit soliton.

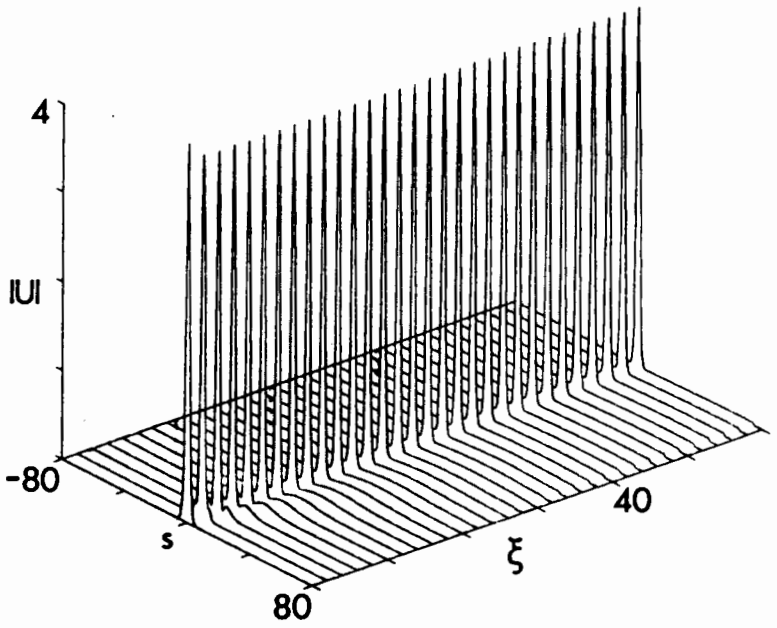

Figure 5.9: Upswitch from G_i to G_f (refer to Figure 5.6 and Table 5.2).

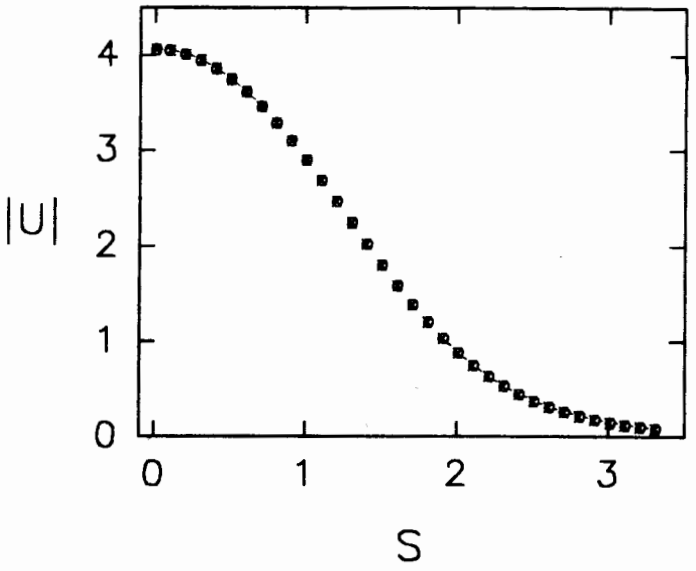

Figure 5.10: Least squares fit of the output pulse from upswitching run G.
x - numerical result
o - best fit soliton.

easily between pulses with very different amplitudes, which appear far apart on the high and low branches of the soliton line.

In conclusion, it can be seen from the results in this chapter that it is possible to switch easily between high and low state bistable solitons of the second kind, for the models under consideration. The high and low states can be chosen to be sufficiently far apart in amplitude that they may be distinguished despite the lack of an unstable gap. Unlike the situation for BISOL1, hysteresis-free back and forth switches are possible for BISOL2. For these reasons, BISOL2 are good candidates for use in optical logic operation.

Chapter 6

Conclusions

Optical solitons can propagate in fibers when the compressing effects of the fiber nonlinearity balance the spreading effects of dispersion. These solitons can be modeled mathematically as solutions to the generalized nonlinear Schrödinger equation (GNLSE). Solitons are extremely narrow and stable, and thus are ideal for communications applications where data must be sent at a high bit rate over very long distances. The information to be transmitted is conventionally represented in binary code, with a pulse representing a one and a gap representing a zero. The phenomenon of soliton bistability allows ones and zeros to be represented instead by "tall" (high state) and "short" (low state) pulses.

Optical fibers may support bright soliton bistability in two ways. Bistable solitons of the *first* kind (BISOL1) exist when solitons may be propagated with the same total energy but different propagation parameters. Bistable solitons of the *second* kind (BISOL2) exist when the fiber supports solitons with the same width but different amplitudes. BISOL2, but not BISOL1, are supported by fibers with nonlinearities

described in the GNLSE by $f = I - \alpha I^2$ and $f = 0.5I(\gamma I + 2)(1 + \gamma I)^{-2}$. These models of fiber nonlinearity qualitatively mimic the behaviour of known classes of materials.

Numerical collision studies of bistable solitons arising from the model $f = I - \alpha I^2$ demonstrate a wide range of possible outcomes. In at least one case, a low-state soliton is one of the output products of a collision between two high-state solitons, a result which suggests that switching between states is possible. The collision studies also indicate that the explicit numerical scheme, which is also used for amplification and switching runs, is a viable way to simulate the GNLSE numerically.

Dark solitons, which take the form of localized "holes" in a constant intensity background, may also exhibit two different forms of bistability. Dark solitons with the same "hole energy" and different "modulation depths" ($D = (I_{\max} - I_{\min})/I_{\max}$) are analogous to bright BISOL1. Several analogies to bright BISOL2 can be developed: dark solitons may have the same width and background intensity, but different depths; the same width and depth, but different backgrounds; or the same width and modulation depth (D), but different backgrounds. By the first of these definitions, the model $f = I - \alpha I^2$ does not support dark soliton bistability. The first definition is, however, the most practical of the three since, in experiment, it is difficult to change the background intensity quickly. The model $f = I - \alpha I^2$ *does* support dark soliton bistability as described by the second and third definitions.

It has been demonstrated previously that it is possible to switch between high

and low state bright BISOL1, by amplifying the soliton pulses. Numerical amplification of bright BISOL2 arising from the above-mentioned models results in a variety of behaviours, including dispersion, oscillation, splitting, and switching. An analytic variational method based on that of Anderson [35] generally predicts the observed behaviour well. However, the variational analysis is not able to account for the switching that occurs for suitably chosen amplifications. This is because its predictions are based on the assumption that the pulse shape does not change dramatically or permanently, whereas significant shape changes usually occur during switching.

Both upswitching (from low to high state) and downswitching (from low to high state) are possible for both models of the fiber nonlinearity. In both models, essentially hysteresis-free back-and-forth switching is observed numerically between BISOL2 states, whereas, for BISOL1, hysteresis-free switching is not generally possible. Fibers with a saturable nonlinearity are likely to be more useful in practice than those modeled by $f = I - \alpha I^2$, as they easily allow switching between solitons of very different amplitudes, which can be distinguished despite the lack of an unstable gap separating the high and low states. Overall, bright BISOL2 appear to have good potential for use in optical switching operations.

Bibliography

[1] R.H.Enns, D.E.Edmundson, S.S.Rangnekar, and A.E. Kaplan. *Optical and Quantum Electron.*, 24:S1295, 1992.

[2] S.L. Eix and R.H. Enns. *Phys. Rev.*, 1993. In press - to be published June 1993.

[3] N.J. Zabusky and M.D. Kruskal. *Phys. Rev. Lett.*, 15:240, 1965.

[4] C.S. Gardner, J.M. Greene, M.D. Kruskal, and R.M. Miura. *Phys. Rev. Lett.*, 19:1095, 1967.

[5] A. Hasegawa. *Optical Solitons in Fibers, 2nd ed.* Springer-Verlag, Berlin, 1990.

[6] G.P. Agrawal. *Nonlinear Fiber Optics.* Academic Press, Inc., San Diego, 1989.

[7] Dwight E. Gray, editor. *American Institute of Physics Handbook.* McGraw–Hill Book Company Ltd., New York, 1963.

[8] G.R. Fowles. *Introduction to Modern Optics.* Dover Publications, Inc., New York, 1975.

[9] J.D. Jackson. *Classical Electrodynamics, 2nd ed.* John Wiley and Sons, New York, 1975.

[10] Akira Hasegawa and Frederick Tappert. *Appl. Phys. Lett.*, 23(3):142, 1973.

[11] Akira Hasegawa and Frederick Tappert. *Appl. Phys. Lett.*, 23(4):171, 1973.

[12] V.E. Zakharov and A.B. Shabat. *Soviet Physics JETP*, 34(1):62, 1972.

[13] V.E. Zakharov and A.B. Shabat. *Soviet Physics JETP*, 37(5):823, 1973.

[14] S.Gatz and J.Herrmann. *J. Opt. Soc. Am.*, B8(11):2296, 1991.

[15] S.Gatz and J.Herrmann. *Optics Lett.*, 17(7), 1992.

[16] Wieslaw Krolikowski and Barry Luther-Davies. *Optics Lett.*, 17(20):1459, 1992.

[17] Stuart Cowan, R.H. Enns, S.S.Rangnekar, and Sukhpal S. Sanghera. *Can. J. Phys.*, 64:311, 1986.

[18] J.Herrmann. *Opt. Comm.*, 87:161, 1992.

[19] Leslie J. Mulder and R.H.Enns. *IEEE J. Quantum Electron.*, 1989.

[20] H. Puell, K. Spanner, W. Falkenstein, W. Kaiser, and C.R. Vidal. *Phys. Rev.*, 14:2240, 1976.

[21] Jean-Louis Coutaz and Martin Kull. *J. Opt. Soc. Am.*, B8(1):8, 1991.

[22] R.H.Enns, S.S.Rangnekar, and A.E.Kaplan. *Phys. Rev.*, A36(3):1270, 1987.

[23] A.Sergio Bezzera Sombra. *Opt. Comm.*, 94:92, 1992.

[24] L.F.Mollenauer, R.H.Stolen, and J.P.Gordon. *Phys. Rev. Lett.*, 45(13), 1980.

[25] P. Emplit, J.P. Hamaide, F. Reynaud, C. Froehly, and A. Barthelemy. *Opt. Comm.*, 62:374, 1987.

[26] D.Krökel, N.J.Halas, G.Giuliani, and D.Grischkowsky. *Phys. Rev. Lett.*, 60(1):29, 1988.

[27] A.M. Weiner, J.P. Heritage, R.J. Hawkins, R.N. Thurston, E.M. Kirschner, D.E. Leaird, and W.J. Tomlinson. *Phys. Rev. Lett.*, 61:2445, 1988.

[28] Neal S. Bergano. *Optics and Photonics News*, January:8, 1993.

[29] S.Gatz and J.Herrmann. *IEEE J. Quantum Electron.*, 28(7):1732, 1992.

[30] A.E.Kaplan. *Phys. Rev. Lett.*, 55(12):1291, 1985.

[31] R.H.Enns and S.S.Rangnekar. *Phys. Rev.*, A45:3354, 1992.

[32] R.H. Enns, D.M. McAvity, and S.S. Rangnekar. *Mathl. Comput. Modelling*, 11:112, 1988.

[33] R.H.Enns and L.J.Mulder. *Optics Lett.*, 14(10):509, 1989.

[34] J.Herrmann. *Opt. Comm.*, 91:337, 1992.

[35] D. Anderson. *Phys. Rev.*, A27:3135, 1983.

[36] R.H. Enns and S.S. Rangnekar. *IEEE J. Quantum Electron.*, QE-23(7):1199, 1987.